

A STUDY ON THE DEACTIVATION OF NICKEL-BASED CATALYST FOR THE DRY  
REFORMING OF METHANE VIA DENSITY FUNCTIONAL THEORY



A Thesis Submitted in Partial Fulfillment of the Requirements  
for the Degree of Master of Engineering in Chemical Engineering

Department of Chemical Engineering

FACULTY OF ENGINEERING

Chulalongkorn University

Academic Year 2019

Copyright of Chulalongkorn University

การศึกษาการเสื่อมสภาพบนตัวเร่งปฏิกิริยาประเภทนิกเกิลในปฏิกิริยารีดอกซ์แบบแห้งของมีเทน  
โดยใช้ทฤษฎีฟังก์ชันนอลความหนาแน่น



วิทยานิพนธ์นี้เป็นส่วนหนึ่งของการศึกษาตามหลักสูตรปริญญาวิทยาศาสตรมหาบัณฑิต  
สาขาวิชาวิศวกรรมเคมี ภาควิชาวิศวกรรมเคมี  
คณะวิศวกรรมศาสตร์ จุฬาลงกรณ์มหาวิทยาลัย  
ปีการศึกษา 2562  
ลิขสิทธิ์ของจุฬาลงกรณ์มหาวิทยาลัย

Thesis Title    A STUDY ON THE DEACTIVATION OF NICKEL-BASED  
    CATALYST FOR THE DRY REFORMING OF METHANE VIA  
    DENSITY FUNCTIONAL THEORY  
By    Mr. Mongkol Lerdpongsiripaisarn  
Field of Study    Chemical Engineering  
Thesis Advisor    SUPAREAK PRASERTHDAM, Ph.D.

---

Accepted by the FACULTY OF ENGINEERING, Chulalongkorn University in  
Partial Fulfillment of the Requirement for the Master of Engineering

..... Dean of the FACULTY OF  
ENGINEERING  
(Professor SUPOT TEACHAVORASINSKUN, Ph.D.)

THESIS COMMITTEE

..... Chairman  
(Professor JOONGJAI PANPRANOT, Ph.D.)

..... Thesis Advisor  
(SUPAREAK PRASERTHDAM, Ph.D.)

..... Examiner  
(Assistant Professor SUPHOT PHATANASRI, Ph.D.)

..... External Examiner  
(Pussana Hirunsit, Ph.D.)

มงคล เลิศพงษ์ศิริไพศาล : การศึกษาการเสื่อมสภาพบนตัวเร่งปฏิกิริยาประเภทนิกเกิล  
 ในปฏิกิริยารีฟอร์มมิงแบบแห้งของมีเทนโดยใช้ทฤษฎีฟังก์ชันนอลความ  
 หนาแน่น . ( A STUDY ON THE DEACTIVATION OF NICKEL-BASED  
 CATALYST FOR THE DRY REFORMING OF METHANE VIA DENSITY  
 FUNCTIONAL THEORY) อ.ที่ปรึกษาหลัก : ดร.ศุภฤกษ์ ประเสริฐธรรม

การประเมินเสถียรภาพของตัวเร่งปฏิกิริยาสำหรับปฏิกิริยารีฟอร์มมิงแบบแห้งของมีเทน  
 ในงานวิจัยนี้จะถูกพิจารณาผ่านประสิทธิภาพของการป้องกันการเกิดโค้กและความสามารถในการ  
 กำจัดโค้ก ประสิทธิภาพของการป้องกันการเกิดโค้กจะถูกพิจารณาผ่านค่าพลังงานการดูดซับ  
 ระหว่างโค้กและตัวเร่งปฏิกิริยา สำหรับหน้าตัด 100 และ 211 ของตัวเร่งปฏิกิริยาโลหะผสม  
 ระหว่างนิกเกิลกับโคบอลต์พบว่ามีค่าพลังงานการดูดซับสูงกว่าตัวเร่งปฏิกิริยานิกเกิล ซึ่งหมายถึง  
 ตัวเร่งปฏิกิริยาโลหะผสมระหว่างนิกเกิลกับโคบอลต์มีความแข็งแรงของพันธะที่อ่อนกว่าตัวเร่ง  
 ปฏิกิริยานิกเกิล สำหรับหน้าตัด 111 ตัวเร่งปฏิกิริยานิกเกิลและตัวเร่งปฏิกิริยาโลหะผสมระหว่าง  
 นิกเกิลกับโคบอลต์มีค่าพลังงานการดูดซับที่ใกล้เคียงกัน อีกทั้งตัวเร่งปฏิกิริยาโลหะผสมระหว่าง  
 นิกเกิลกับโคบอลต์มีค่าพลังงานการดูดซับที่สูงกว่าตัวเร่งปฏิกิริยาแบบโลหะมีสกุล ได้แก่ โรเดียม  
 และแพลเลเดียม ซึ่งหมายความว่าตัวเร่งปฏิกิริยาโลหะผสมระหว่างนิกเกิลกับโคบอลต์มี  
 ประสิทธิภาพในการป้องกันโค้กที่เทียบเท่าได้กับตัวเร่งปฏิกิริยาแบบโลหะมีสกุล ความสามารถในการ  
 กำจัดโค้กสามารถพิจารณาผ่านค่าพลังงานก่อกัมมันต์ของการเคลื่อนไหวของโค้กบนผิวตัวเร่ง  
 ปฏิกิริยาหรือการหลุดของโค้กจากตำแหน่งกัมมันต์ที่เสถียรที่สุดไปยังตำแหน่งกัมมันต์อื่น สำหรับ  
 หน้าตัด 100 ของตัวเร่งปฏิกิริยานิกเกิลและตัวเร่งปฏิกิริยาโลหะผสมระหว่างนิกเกิลกับโคบอลต์มี  
 พบว่าในพื้นผิวนี้มีตำแหน่งกัมมันต์เพียงแค่ตำแหน่งเดียวทำให้ไม่สามารถเกิดการหลุดของโค้กจาก  
 ตำแหน่งกัมมันต์ตำแหน่งหนึ่งและไปเกาะอีกไปที่ตำแหน่งกัมมันต์ตำแหน่งหนึ่งได้ สำหรับหน้าตัด  
 111 และ 211 ของตัวเร่งปฏิกิริยานิกเกิลและตัวเร่งปฏิกิริยาโลหะผสมระหว่างนิกเกิลกับโคบอลต์  
 มีพบว่าตัวเร่งปฏิกิริยาโลหะผสมระหว่างนิกเกิลกับโคบอลต์มีแสดงค่าพลังงานก่อกัมมันต์ที่น้อยกว่า  
 ตัวเร่งปฏิกิริยานิกเกิล ซึ่งหมายความว่าตัวเร่งปฏิกิริยาโลหะผสมระหว่างนิกเกิลกับโคบอลต์มี  
 สามารถแสดงประสิทธิภาพของการกำจัดโค้กได้ดีกว่าตัวเร่งปฏิกิริยานิกเกิล

สาขาวิชา วิศวกรรมเคมี

ลายมือชื่อนิสิต .....

ปีการศึกษา 2562

ลายมือชื่อ อ.ที่ปรึกษาหลัก .....

# # 6170245721 : MAJOR CHEMICAL ENGINEERING

KEYWORD: DFT, NiCo, DRM

Mongkol Lerdpongsiripaisarn : A STUDY ON THE DEACTIVATION OF NICKEL-BASED CATALYST FOR THE DRY REFORMING OF METHANE VIA DENSITY FUNCTIONAL THEORY. Advisor: SUPAREAK PRASERTHDAM, Ph.D.

In this work, the stability assessment of catalyst for the dry reforming reaction was investigated through the coke resistance performance and the ability of coke removal. The coke resistance performance was considered via the coke adsorption energy. For surface 100 and 211, NiCo bimetallic catalyst and Ni exhibit weaker bonding between coke and catalyst surface. For surface 111, both catalysts exhibited similar adsorption energy value. NiCo bimetallic catalyst also showed higher adsorption energy for surface 111 and 211 than the noble metal catalyst such as Rh and Pd catalyst which means NiCo catalysts can show the coke resistance performance that is comparable with the noble metal catalyst. The ability of coke removal was investigation through the activation of the coke movement on catalyst surface or coke diffusion from the most stable active site to another stable active site. For surface 100 of Ni and NiCo catalyst, there is only one stable active site that refers there is no coke movement on surface 100. For surface 111 and 211, NiCo catalyst shows lower activation energy of coke movement than Ni catalyst that translates NiCo is the better performance catalyst for coke removal.

Field of Study: Chemical Engineering

Student's Signature .....

Academic Year: 2019

Advisor's Signature .....

## ACKNOWLEDGEMENTS

I would like to express my sincere thanks to my advisor, Dr. Supareak Praserttham, for invaluable suggestions and constant encouragement to do this research. His guideline helps me throughout the tough times of researching.

I also would like to thank Professor Dr. Joongjai Panpranot, as the chairman, Assistant Professor Dr. Suphot Phatanasri and Dr. Pussana Hirunsit, as the committee member of the thesis for their valuable time, suggestions and comments

The author thanks the Center of Excellence on Catalysis and Catalytic Reaction Engineering, High-Performance Computing Unit, Department of Chemical Engineering, Faculty of Engineering, Chulalongkorn University, for financial support.

Moreover, I also would like to thank, Dr. Tinnakorn Saelee and Dr. Meena Rittirum, postdoctoral of my advisor, who give me knowledge, enjoyable times, and their comments and suggestion.

Finally, I most gratefully acknowledge my beloved parent, family, and friends for all their support and encouragement.



จุฬาลงกรณ์มหาวิทยาลัย  
CHULALONGKORN UNIVERSITY

Mongkol Lerdpongsiripaisarn

## TABLE OF CONTENTS

	Page
.....	iii
ABSTRACT (THAI).....	iii
.....	iv
ABSTRACT (ENGLISH).....	iv
ACKNOWLEDGEMENTS.....	v
TABLE OF CONTENTS.....	vi
LIST OF TABLES.....	ix
LIST OF FIGURES.....	xi
CHAPTER I.....	1
INTRODUCTION.....	1
1.1 Introduction.....	1
1.2 Objective.....	3
1.3 The scope of the research.....	3
1.4 Research Methodology.....	3
CHAPTER II BACKGROUND AND LITERATURE REVIEWS.....	5
2.1 Nickel.....	5
2.2 Cobalt.....	5
2.3 Methane.....	6
2.4 Carbon dioxide.....	7
2.5 Dry reforming of methane.....	7
2.6 Coke.....	8

2.7 Density theory functional (DFT).....	9
2.6 Vibrational frequency.....	12
2.7 Literature reviews.....	14
CHAPTER III COMPUTATIONAL DETAILS .....	16
3.1 The bulk optimization calculation.....	16
3.2 The adsorption energy analysis.....	16
3.3 The coke mobility analysis .....	17
3.4 Rate of coke diffusion .....	17
CHAPTER IV RESULTS AND DISCUSSION .....	19
4.1 Bulk optimization .....	19
4.2 Structure optimization .....	20
4.3 Coke adsorption on the catalyst surface .....	22
4.4 Adsorption properties of catalyst surfaces .....	28
4.5 Coke movement on the catalyst surface.....	30
4.6 Rate of coke diffusion .....	32
4.7 Design and guideline of catalyst.....	34
CHAPTER V.....	36
CONCLUSION .....	36
APPENDIX.....	37
APPENDIX A      CALCULATON FOR ADSORPTION ENERGY .....	38
APPENDIX B      CALCULATON FOR ADSORPTION ENERGY .....	39
APPENDIX C      CALCULATON FOR RATE OF COKE DIFFUSION .....	40
APPENDIX D      MATLAB CODE FOR RATE OF COKE DIFFUSION CALCULATION.....	48
REFERENCES .....	53



VITA..... 55



จุฬาลงกรณ์มหาวิทยาลัย  
**CHULALONGKORN UNIVERSITY**

## LIST OF TABLES

	Page
Table 1 Properties of Nickel.....	5
Table 2 Properties of Cobalt .....	6
Table 3 Properties of Methane .....	6
Table 4 Properties of Carbon dioxide.....	7
Table 5 Forms and Reactivities of Carbon Species Formed .....	8
Table 6 The possible active sites and adsorption sites of 1 <sup>st</sup> carbon adsorption on Ni(100), Ni(111), Ni(211), NiCo(100), NiCo(111), and NiCo(211) catalysts. ....	22
Table 7 Adsorption energies of 1 <sup>st</sup> carbon adsorption on adsorption sites of Ni(100), Ni(111), Ni(211), NiCo(100), NiCo(111), and NiCo(211) catalysts. ....	26
Table 8 Adsorption energies of 1 <sup>st</sup> , 2 <sup>nd</sup> , and 3 <sup>rd</sup> carbon adsorption on Ni(100), Ni(111), Ni(211), NiCo(100), NiCo(111), and NiCo(211) surfaces catalysts.....	27
Table 9 Adsorption energies of 1 <sup>st</sup> , 2 <sup>nd</sup> , and 3 <sup>rd</sup> carbon adsorption on Ni(100), Ni(111), Ni(211), NiCo(100), NiCo(111), and NiCo(211) surfaces catalysts.....	27
Table 10 Equilibrium adsorption height ( $d_{c-sur}$ ) of 1 <sup>st</sup> carbon adsorption on Ni(100), Ni(111), Ni(211), NiCo(100), NiCo(111), and NiCo(211) surfaces catalysts.....	28
Table 11 The d-band center ( $\epsilon_d$ ) at the top surface for Ni and Co on Ni, Co.....	29
Table 12 The activation energies for the forward ( $E_{a,f}$ ) and reverse ( $E_{a,r}$ ) for coke movement reaction on Ni(100), Ni(111), Ni(211), NiCo(100), NiCo(111), and NiCo(211) surfaces catalysts.....	32
Table 13 Vibrational frequency of Initial state (Hcp).....	40
Table 14 Vibrational frequency of transition state.....	41
Table 15 Vibrational frequency of final state (Fcc).....	42
Table 16 $Q_{vib}$ and $E_{ZPE}$ of the initial state, transition state and final state .....	44

Table 17 the results of Forward rate constant and Reverse rate constant of Ni, Co,  
and NiCo catalyst..... 46



## LIST OF FIGURES

	Page
Figure 1 Overview of greenhouse gas emission in 2017 (Left) and Source of greenhouse gas emission in 2017 (Right) .....	1
Figure 2 Formation, transformation, and gasification of carbon on nickel .....	9
Figure 3 Potential energy surface (PES) model [16].....	13
Figure 4 ENCUT and KPOINTS convergence test.....	20
Figure 5 structure of surface (a) 100, (b) 111, and (c) 211 models.....	21
Figure 6 Possible active sites of (a) Ni(100), (b) Ni(111), (c) Ni(211), (d) NiCo(100), (e) NiCo(111), and (f) NiCo(211) surfaces catalysts.....	21
Figure 7 The most stable configuration of 1 <sup>st</sup> , 2 <sup>nd</sup> , and 3 <sup>rd</sup> coke adsorption on (a-c) Ni(100) and (d-f) NiCo(100) .....	24
Figure 8 The most stable configuration of 1 <sup>st</sup> , 2 <sup>nd</sup> , and 3 <sup>rd</sup> coke adsorption on (a-c) Ni(111) and (d-f) NiCo(111) .....	24
Figure 9 The most stable configuration of of 1 <sup>st</sup> , 2 <sup>nd</sup> , and 3 <sup>rd</sup> coke adsorption on (a-c) Ni(211) and (d-f) NiCo(211) .....	25
Figure 10 The total rate of coke diffusion under 1000 K at (a) beginning step, (b) intermediate step, and (c) final step.....	34
Figure 11 the NiCo bimetallic model .....	34

# CHAPTER I

## INTRODUCTION

### 1.1 Introduction

Nowadays, global climate change is the world-class problems. It has gained attention from many countries since it is the main factor making the average world temperature rise, which significantly affects multifarious such as increasing mean sea level, extinction of some animal or plant species, and others. The significant motives are greenhouse gases (GHG) such as Carbon dioxide (CO<sub>2</sub>), Methane (CH<sub>4</sub>), Nitrous oxide (N<sub>2</sub>O), and others.

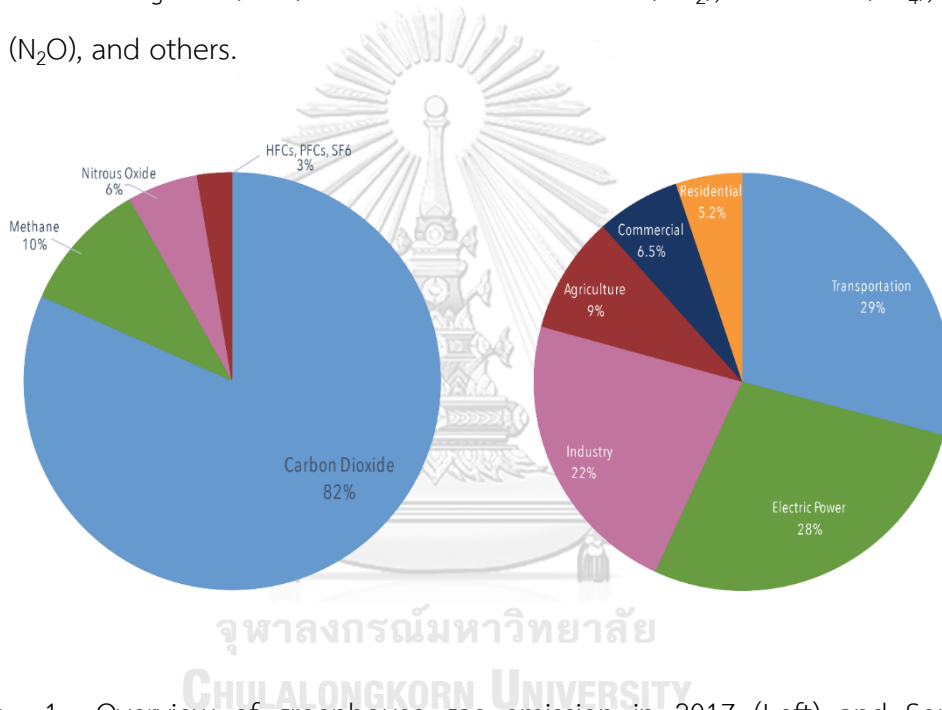


Figure 1 Overview of greenhouse gas emission in 2017 (Left) and Source of greenhouse gas emission in 2017 (Right)

(Source: Inventory of U.S. Greenhouse Gas Emissions and Sinks 1990-2017, 2019)

The primary source of greenhouse gases (Figure 1.1) comes from routine human activities such as transportation, household electricity, and others. These activities release a lot of CO<sub>2</sub>, which is the most gas emission of carbon dioxide.



Dry reforming of methane process (DRM) (Eq.1) is one of the most reactions solving the global warming problem for the reason that it can reduce  $\text{CO}_2$  and  $\text{CH}_4$  that is the most quantity of greenhouse gases and convert into the hydrogen ( $\text{H}_2$ ) and carbon monoxide (CO). DRM also can be value-added chemicals through the other processes such as The Fischer–Tropsch process (Eq.2), which convert CO and  $\text{H}_2$  into liquid hydrocarbons [1]. At present, hydrogen power has gained much attention for the reason that it is green energy, high performance of burning. Also, it can be used for the energy of car, plane, and fuel cell or electrochemical cells that convert hydrogen to electricity power.

For the DRM process, one of the most critical factors affecting DRM is the catalyst. There are many types of metal catalysts using in DRM. Almost catalysts perform the high activity and high coke resistance by using the noble metal, e.g., rhodium (Rh), palladium (Pd), and others [2, 3]. On the other hand, noble metals are not suitable due to there are expensive for industrial scale. Ni catalyst is an alternative catalyst that can fulfill the drawback of noble metal catalyst since it shows high reactivity of DRM comparable to noble metal catalyst[4]. On the other hand, Ni also produces a high rate of coke formation, making a high rate of deactivation [5].

The metal doping in the Ni-based catalyst to form a bimetallic catalyst is a promising way due to its synergetic effect. Each metal doping can improve performance on Ni-based catalysts. The doping Co is an exciting way due to it can improve coke resistance and also showed high reactivity of Ni-based catalyst [6, 7].

Density functional theory (DFT) is an interesting way that has been widely used to analyze the performance of the catalyst. It also showed high reliability due to DFT can calculate the atom behavior, reaction energy, electronic properties, an energy barrier that is difficult to obtain from experimental [8].

In this work, the effect of adding Co into Ni-based catalysts on (1) the performance of coke resistance studied through the coke adsorption on the Ni and NiCo bimetallic catalyst in terms of all configurations of the carbon atom, (2) the ability of coke removal considered through coke movement on the catalyst surface as well as the possible mechanism pathways of carbon diffusion in various position via DFT.

## 1.2 Objective

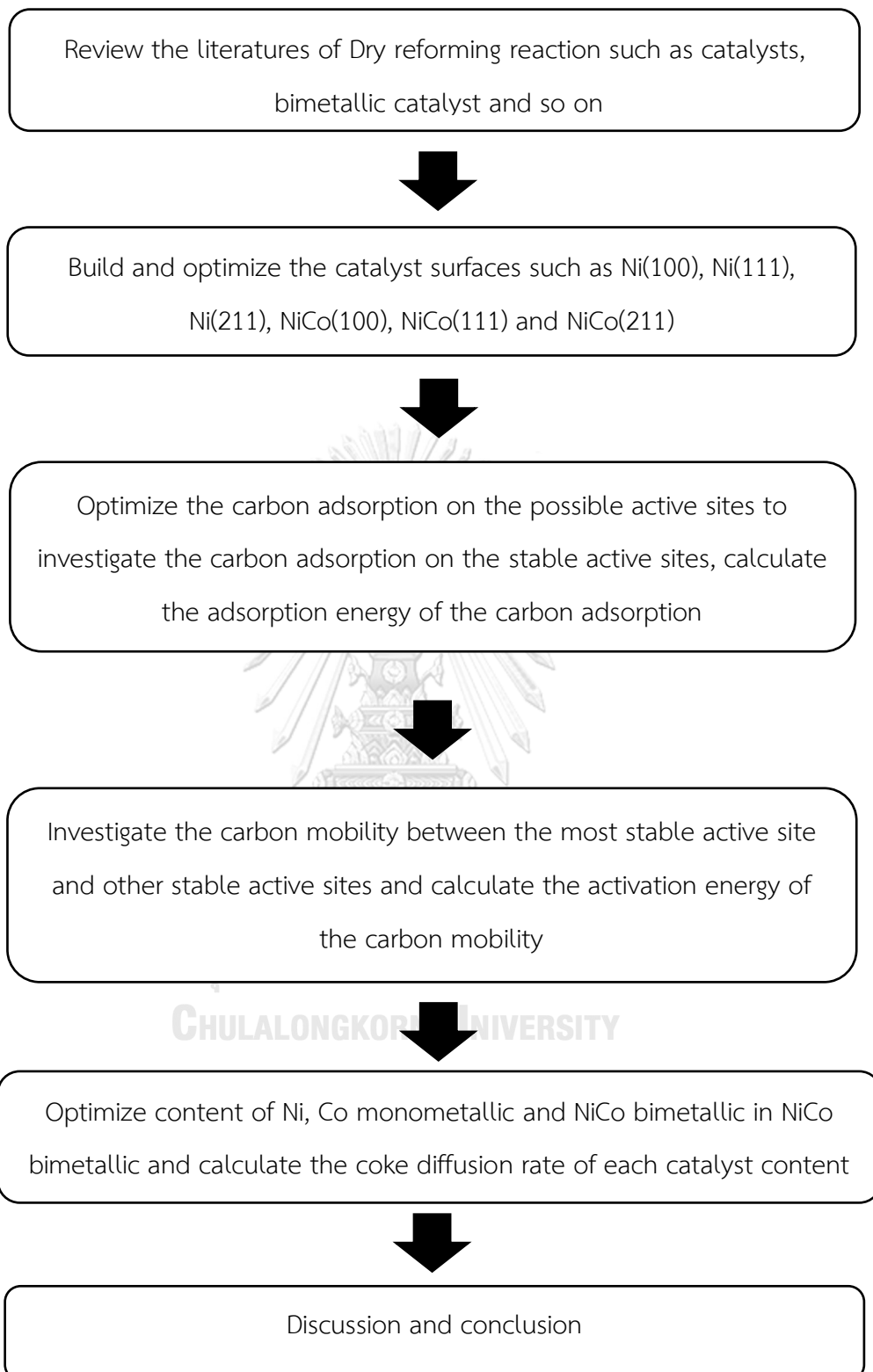
To study the roles of Co in the Ni-based catalyst on the improved coke-resistance in dry reforming of methane (DRM) via density functional theory (DFT).

## 1.3 The scope of the research

The detail of scope research given below:

1. Study the strength of atomic coke (alpha carbon) adsorption on the Ni monometallic catalysts: Ni(100), Ni(111), and Ni(211) surfaces comparing to NiCo bimetallic catalysts: NiCo(100), NiCo(111) and NiCo(211) surfaces
2. Study the coke removal represented by the activation energy of alpha carbon diffusion on Ni monometallic and NiCo bimetallic catalysts

## 1.4 Research Methodology





## CHAPTER II

### BACKGROUND AND LITERATURE REVIEWS

#### 2.1 Nickel

Nickel (Ni) is a chemical element with atomic number 28. The periodic table show Ni is part of group 10 or group VIII B, and period four known as a transition metal, Ni is solid in room temperature, durable, shiny, silvery-white, and moderately good conductor for heat and electricity. Ni can be used in many industrial, whether it be stainless steel, coatings, batteries, catalyst, and others [9].

Table 1 Properties of Nickel

Properties	Values
Chemical formula	Ni
Molecular weight	58.693 g/mol
Density	8.908 g/cm <sup>3</sup>
Melting point	1728 K
Boiling point	3003 K
Crystal structure	face-centered cubic (fcc)
Atomic radius	124 pm

#### 2.2 Cobalt

Cobalt (Co) is a chemical element with atomic number 27. Co can be found in the only crust of the earth. The periodic table show Ni is part of group 9 or group VIII B and period four, which is fragile, hard, silver, and grey. At present, Co can be applied in alloys, batteries, and also a catalyst [10].

Table 2 Properties of Cobalt

Properties	Values
Chemical formula	Co
Molecular weight	58.933 g/mol
Density	8.90 g/cm <sup>3</sup>
Melting point	1768 K
Boiling point	3200 K
Crystal structure	hexagonal close-packed (hcp)
Atomic radius	125 pm

### 2.3 Methane

Methane (CH<sub>4</sub>) is a hydrocarbon or organic compound with a tetrahedral structure with four equivalent C–H bonds. CH<sub>4</sub> is one of the greenhouse gas (GHG). Almost all of CH<sub>4</sub> is found on both ground and undersea. CH<sub>4</sub> is a colorless and unscented gas at ambient temperature. CH<sub>4</sub> has been used as a fuel of household appliances, a turbine, and also used to be chemical feedstock [11].

Table 3 Properties of Methane

Properties	Values
Chemical formula	CH <sub>4</sub>
Molecular weight	16.043 g/mol
Density	0.657 g/L (gas, 25 °C, 1 atm) 0.717 g/L (gas, 0 °C, 1 atm) 422.62 g/L (liquid, -162 °C)
Melting point	90.4 K
Boiling point	111.65 K

## 2.4 Carbon dioxide

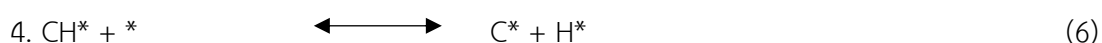
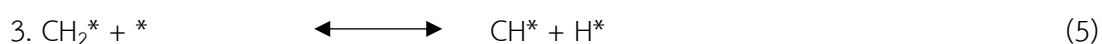
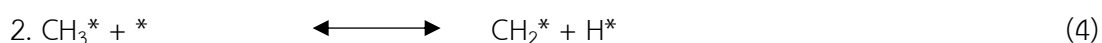
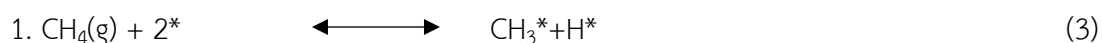
Carbon dioxide (CO<sub>2</sub>) is a covalently double bond of carbon with two oxygen. Almost CO<sub>2</sub> occurred from human activity, e.g., fossil burning, transportation, and others. CO<sub>2</sub> is the most greenhouse gas emission, which is the main cause of making climate change. However, CO<sub>2</sub> can be used in a chemical process, e.g., dry reforming reaction. CO<sub>2</sub> also positively influence on human due to it is the part of plant growth which produce oxygen for human breathing.

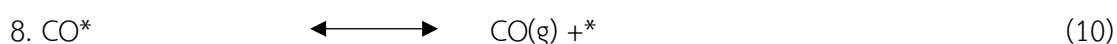
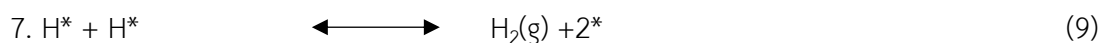
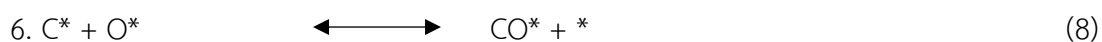
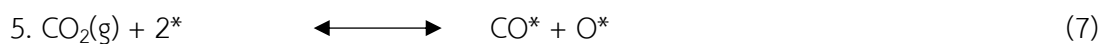
Table 4 Properties of Carbon dioxide

Properties	Values
Chemical formula	CO <sub>2</sub>
Molecular weight	44.009 g/L
Density	1562 kg/m <sub>3</sub> (solid at 1 atm and -78.5 °C) 1101 kg/m <sub>3</sub> (liquid at saturation -37°C) 1.977 kg/m <sub>3</sub> (gas at 1 atm and 0 °C)
Melting point	216.6 K
Critical temperature	304.2 K
Critical pressure	73.8 bar

## 2.5 Dry reforming of methane

Dry reforming of methane is reaction converting CO<sub>2</sub> and CH<sub>4</sub> of ratio 1:1 into the synthesis gas or CO and H<sub>2</sub>. The mechanism of dry reforming reaction may be represented by:





$\text{CH}_4$  cracking (Eq.3) and  $\text{CO}_2$  cracking (Eq.7) are the main reactions of DRM. The  $\text{CH}_x$  dissociation (Eq.4-6) that Eq.4 is the main reaction producing the coke on the catalyst surface. The oxidation of carbon reaction (Eq.8) is the main reaction removing the coke from the catalyst surface [12].

## 2.6 Coke

Coke is a carbonaceous substance of many scales and various kinds, such as encapsulating film, Whisker-like, Pyrolytic carbon, and others. Coke has various effects on the catalyst, whether it be blockage of the active site, plug the pore of the support, and cumulative coke on the wall of the pore of catalyst make stress, which can break up catalyst. Types of coke form also depend on temperature range as shown in Table 5 [13] and transformation of carbon shown in Figure 2 [14]

Table 5 Forms and Reactivities of Carbon Species Formed

Carbon structure	Symbol	Temperature range (°C)
Carbon atomic	$\text{C}_\alpha$	200-400
Polymeric and amorphous films or filaments	$\text{C}_\beta$	250-500
Vermicular filaments, fibers, and whiskers	$\text{C}_\nu$	300-1000
Nickel carbide	$\text{C}_\gamma$	150-250
Graphitic (crystalline) platelets or films	$\text{C}_c$	500-550

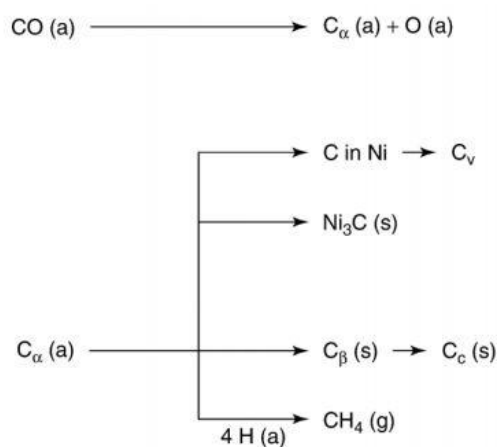


Figure 2 Formation, transformation, and gasification of carbon on nickel

## 2.7 Density theory functional (DFT)

DFT is a quantum mechanical theory for solving many-body problems of physical problems. DFT started from Erwin Schrödinger, who discovered the Schrödinger equation, which is a mathematic equation describing the physical properties of quantum phenomena and wave function movement. However, it can be solved exactly only for one atom (hydrogen atom), and it can be solved for multi-electron systems. Time-independent Schrödinger equation is shown in the following this equation ( $\hat{H}$  = Hamiltonian operator,  $\Psi$  = wave function, and  $E$  = energy of the system)

$$\hat{H}\Psi = E\Psi \quad (11)$$

The equation can be used for solving in one dimension that described by a function of the wave function, which depends on electron position ( $r$ ). Time-independent Schrödinger general equation can be rewritten equation shown in the following equation

$$\hat{H}(r)\Psi(r) = E(r)\Psi(r) \quad (12)$$

Hamiltonian is the sum of the kinetic and potential energy in the system shown in the following equation (  $T$  = kinetic energy in the function of momentum is written as ( $V$  = potential energy in the function of space coordinate,  $p$  = momentum,  $m$  = electron mass,  $Z$  = atomic number,  $e$  = electron charge,  $r$  = distance between electron and nucleus and  $\epsilon_0$  = electric constant.)

$$\hat{H} = \hat{T} + \hat{V} \quad (13)$$

$$\text{where } \hat{T} = \frac{\hat{p}^2}{2m}$$

According to Schrödinger equation has coulomb force between electron, which makes it has to calculate by Numerical. From coulombs' law, the potential equation can be written as:

$$\hat{V} = -\frac{Ze^2}{4\pi r\epsilon_0} \quad (14)$$

the most mutual appearance is the nonrelativistic Schrödinger equation that the quantum mechanics without effects of special relativity can be written as:

For a particle in one dimension, the Hamiltonian is

$$\hat{H} = \frac{\hat{p}^2}{2m} + \hat{V}(x) \quad (15)$$

$$\text{Where } \hat{p} = -i\hbar \frac{d}{dx}$$

Represent into the general form can be written as:

$$\left[ -\frac{\hbar^2}{2m} \frac{d^2}{dx^2} + \hat{V}(x) \right] \psi(x) = E\psi(x) \quad (16)$$

For a particle in three dimensions, the Hamiltonian is

$$\hat{H} = \frac{\hat{p} \cdot \hat{p}}{2m} + V(r) \quad (17)$$

$$\text{Where } \hat{p} = -i\hbar \vec{\nabla},$$

Represent into a general form can be written as:

$$\left[ -\frac{\hbar^2}{2m} \vec{\nabla}^2 + V(r) \right] \psi(r) = E\psi(r) \quad (18)$$

For many body systems or multi-electron Hamiltonian ( $\hbar$  = reduce Planck constant  $= \frac{h}{2\pi}$  , h =Planck constant, M = nuclear mass, m = electron mass, R = distance between nuclear and reference point, r = distance between electron and reference point

$$H = -\sum_{i=1}^N \frac{\hbar^2}{2Mi} \vec{\nabla}_{Ri}^2 + \frac{1}{2} \sum_{i=1}^N \sum_{j=1, i \neq j}^N \frac{Z_i Z_j e^2}{|R_i - R_j|} - \frac{\hbar^2}{2m} \sum_{i=1}^n \vec{\nabla}_{r_i}^2 - \sum_{i=1}^N \sum_{j=1}^n \frac{Z_i e^2}{|R_i - r_j|} + \frac{1}{2} \sum_{i=1}^n \sum_{j=1, i \neq j}^n \frac{e^2}{|r_i - r_j|} \quad (19)$$

The kinetic energy of nuclear can be written as:

$$-\sum_{i=1}^N \frac{\hbar^2}{2Mi} \vec{\nabla}_{Ri}^2 \quad (20)$$

The kinetic energy of electron can be written as:

$$-\frac{\hbar^2}{2m} \sum_{i=1}^n \vec{\nabla}_{r_i}^2 \quad (21)$$

The potential energy of nuclear can be written as:

$$\frac{1}{2} \sum_{i=1}^N \sum_{j=1, i \neq j}^N \frac{Z_i Z_j e^2}{|R_i - R_j|} \quad (22)$$

The potential energy of electron - electron interaction can be written as:

$$-\sum_{i=1}^N \sum_{j=1}^n \frac{Z_i e^2}{|R_i - r_j|} \quad (23)$$

The potential energy of nuclear – electron interaction can be written as:

$$\frac{1}{2} \sum_{i=1}^n \sum_{j=1, i \neq j}^n \frac{e^2}{|r_i - r_j|} \quad (24)$$

In 1927, Max Born and J. Robert Oppenheimer approached the Born-Oppenheimer approximation describing the quantum states of molecules. According to the mass of an electron is about  $9.1 \times 10^{-31}$  kg, and a mass of a neutron is about  $1.67 \times 10^{-27}$  kg. The difference between the mass of them is massive (more than 1,800 times) that the mass of an electron is greater than the mass of a neutron. The kinetic energy of ions term is neglected since the kinetic energy of an electron is much higher than it that makes the nuclear move much slower than electrons seems like

ions are immobile. The Born-Oppenheimer approximation proved that the potential of nuclear is a function of nuclear motion that makes the potential energy of nuclear is neglect. From the Born-Oppenheimer approximation, the Hamiltonian can be written as:

$$H = -\frac{\hbar^2}{2m} \sum_{i=1}^n \vec{\nabla}_{r_i}^2 - \sum_{i=1}^N \sum_{j=1}^n \frac{Z_i e^2}{|R_i - r_j|} + \frac{1}{2} \sum_{i=1}^n \sum_{j=1, i \neq j}^n \frac{e^2}{|r_i - r_j|} \quad (25)$$

Kohn sham Equation is the one-electron Schrödinger equation of a fabricated system of non-interacting particles that generate the same density of all interacting particles

Kohn sham Equation for a single particle can be written as:

$$\left[ -\frac{\nabla^2}{2} + V_n(r) + V_H(r) + V_x(r) + V_c(r) \right] \phi_i(r) = \varepsilon_i \phi_i(r) \quad (26)$$

Where  $V_c$  = Correlation potential,  $V_H$  = Hartree - Fock potential,  $V_x$  = Exchange-potential

The hamiltonian equation for many particles can be written as:

$$H(r_1, r_2, \dots, r_N) = -\sum_i \frac{\nabla_i^2}{2} + \sum_i V_n(r) + \frac{1}{2} \sum_{i \neq j} \frac{1}{|r_i - r_j|} \quad (27)$$

## 2.6 Vibrational frequency

After running the transition state structure, it is necessary to verify the transition state structure and stable structure through the vibrational frequency was considered through the potential energy surface, as shown in Figure 3, for the stable structure or a minimum point on the potential energy surface. All of the normal-mode force constants are positive. Each vibrational mode is a restoring force like a spring. When the atom moves from the minimum point, there is a restoring force to pull that atom move to the minimum point in the opposite direction. For the transition state, one of all vibrational modes is different. The motion of the atom takes the transition state toward the second structure or the first structure. This motion is without a restoring force. This vibrational mode takes place through the transition state on a one-way, the force constant is the first derivative of the gradient,



along the reaction coordinate the surface slopes downward. Thus, the force constant is negative. The vibrational frequency is calculated following this equation

$$\tilde{\nu} = \frac{1}{2\pi c} \left( \frac{k}{\mu} \right)^{1/2} \quad (28)$$

Where  $\tilde{\nu}$  is a vibrational frequency,  $c$  denotes the velocity of light,  $k$  is force constant,  $\mu$  is reduced mass of the molecule

According to the vibrational frequency is calculated from the square root of the force constant. The transition state must have exactly one imaginary frequency or called “a first-order saddle point.” It means one of the vibrational eigenvalues will be negative, which means that the changing configuration way has only one direction, and there is the maximum energy [15].

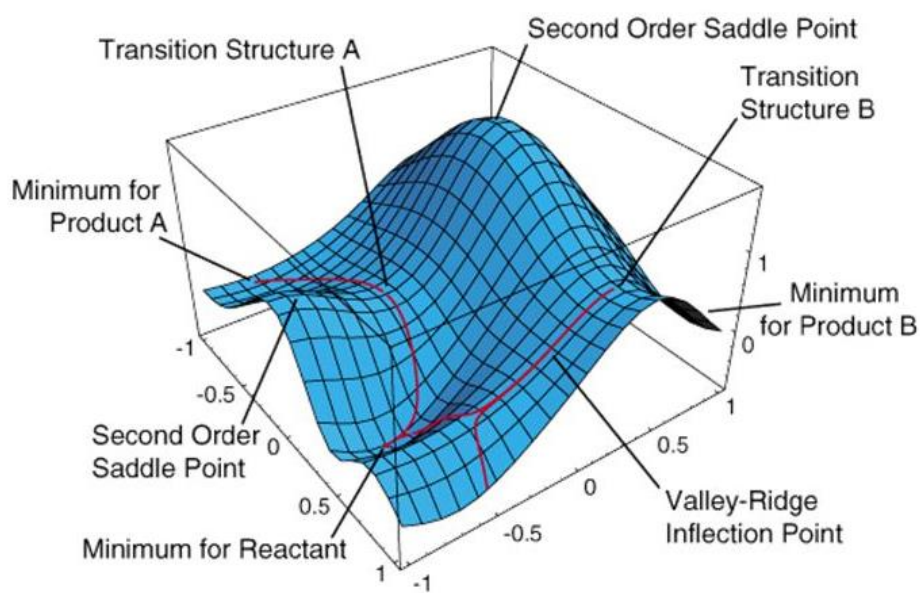


Figure 3 Potential energy surface (PES) model [16]

## 2.7 Literature reviews

Tsyganok et al. (2003) [17] demonstrated using supported noble metal catalysts in DRM. The noble metals used in the experiment supported on Mg–Al mixed oxide at temperature 800 degrees Celsius. The results showed almost noble metal catalyst exhibited high conversion and selectivity. Especially Ru, Rh, and Ir supported on Mg–Al mixed oxide reached conversion of CH<sub>4</sub> and CO<sub>2</sub> more than 90% and 95%, respectively. Also, those catalysts got selectivity of H<sub>2</sub> and CO at about 98%. Notably, the amount of coke deposited occurred on Rh and Ru supported on Mg–Al mixed oxide catalysts was less than 2%wt.

Shamsi (2002) [4] used Ni-based and noble metal catalysts on dry methane reforming. The results showed that the activity of Ni-based and noble metal catalysts was comparable in the initial time at temperature 800 degrees Celsius. Therefore, it can be implied by the stability of the noble metal catalysts were higher than Ni-based catalyst. The deactivation of Ni-based catalysts causes carbon deposition that plugged the reactor; on the other hand, Rh catalyst produced little or no carbon deposition on the catalyst and also used low metal loading.

Son et al. (2014) [18] studied coke formation on Ni/ $\gamma$ -Al<sub>2</sub>O<sub>3</sub> catalyst for DRM by using the weight of the initial catalyst was 0.6g at temperature was 850 degrees Celsius. The initial conversion of CH<sub>4</sub> was 96.5% and rapidly deactivated until the conversion of CH<sub>4</sub> was 81.2%. Besides, the BET surface area was readily decreased from 144.8 m<sup>2</sup>/g at an initial time until 57.1 m<sup>2</sup>/g. The TGA method used for the investigated amount of deposited coke that the removal of deposited coke of catalyst was about 0.46 g. The TEM images proved that the coke formation type was whisker carbon, which is the primary reaction for quick termination of DRM over Ni/ $\gamma$ -Al<sub>2</sub>O<sub>3</sub> catalyst.

Bian et al (2017) [19] reviewed metal added in Ni-based to form the bimetallic catalyst for dry reforming of methane. Each metal added in Ni-based catalyst showed different improvement of performance. Adding noble metal such as

Pt, Rh, and Ru was remarkable in activity improvement of DRM and slightly decreasing coke formation of catalyst. Ni-based added Co form Bimetallic Ni-Co catalysts were outstanding the improvement of coke resistance, decreasing or elimination of coke formation.

Liu et al. (2019) [6] reported the increased stability of Ni-Co bi-metallic over dry reforming. The monometallic Ni, Co, and bi-metallic Ni-Co supported on  $\gamma$ -Al<sub>2</sub>O<sub>3</sub> – HY zeolite. The CO chemisorption results showed the bi-metallic has the highest number of active sites and metal dispersion. From the peak in H<sub>2</sub>, TPR profiles of the catalyst can be described as the bi-metallic showed a peak at the highest temperature, which means the bi-metallic was the strongest interaction between metal and support. The bi-metallic showed the highest conversion of CH<sub>4</sub> and CO<sub>2</sub>, the high selectivity of H<sub>2</sub>, and also decreasing the amount of coke deposited from Ni/ $\gamma$ -Al<sub>2</sub>O<sub>3</sub> – HY zeolite catalyst.

Niu et al. (2020) [20] studied the ability of the elementary reaction of dry reforming of methane of Ni(111), Pt(111), and Ni@Pt(111) catalyst through the activation energies. There are two types of methane cracking reaction are direct methane cracking, and O/OH assisted methane cracking. The direct methane cracking was found that Ni(111) exhibited the lowest activation energy, which means the most accessible catalyst to activate the reaction. On the other hand, For O/OH assisted methane cracking, Ni@Pt(111) exhibited the lowest activation energy. In the part of the coke reaction, which takes to consider the stability of the catalyst, considered two parts are coke formation and coke removal reaction. For coke formation was found, Ni(111) showed the lowest activation. Conversely, in part of the coke removal reaction was found Ni@Pt(111) exhibited the lowest activation. It can be concluded that Ni@Pt(111) showed the best stability out of 3 catalysts hence showed the best performance for coke removal and coke resistance.

## CHAPTER III

### COMPUTATIONAL DETAILS

#### 3.1 The bulk optimization calculation

3.1.1 The cutoff energy (ENCUT) – Optimize with the different ENCUT within the range 100 to 700 step by 50 at fixed the 8x8x8 Monkhorst-Pack k-mesh Brillouin-zone (KPOINTS) integration were used.

3.1.2 Monkhorst-Pack k-mesh Brillouin-zone (KPOINTS) – Optimize with the different KPOINTS within the range 1x1x1 to 8x8x8 step by 1 and fixed the ENCUT from step 3.1.1

3.1.3 set the other parameters such as force converged of 0.05 eV/Å, energy convergence of  $1.0 \times 10^{-6}$  eV/atom.

#### 3.2 The adsorption energy analysis

3.2.1 Build the surface slab and investigate all the possible active sites that carbon can adsorb on the Ni(100), Ni(111), Ni(211), NiCo(100), NiCo(111), and NiCo(211) surfaces.

3.2.2 Optimize all the possible active sites that carbon can adsorb to examine the stable active sites.

3.2.3 Calculate the adsorption energy (Eads) follows the equation:

$$E_{ads} = E_{complex} - (E_{coke} + E_{surface}) \quad (29)$$

where  $E_{complex}$  is the total energy of the adsorption complex (C atom on catalyst surfaces),  $E_{coke}$  is the total energy of isolate coke in a vacuum and  $E_{surface}$  is the total energy of the clean surfaces before adsorption.

3.2.4 Verify the stable structure through the vibrational frequency.

3.2.5 Discuss the results through the most stable active site to be a representative active site of each slab.

### 3.3 The coke mobility analysis

3.3.1 Investigate all the pathways of coke mobility between the most stable active site and other stable active sites that carbon adsorbs on the Ni(100), Ni(111), Ni(211), NiCo(100), NiCo(111), and NiCo(211) surfaces.

3.3.2 Calculate the activation energy of coke diffusion from the stable active site to other stable active sites that carbon adsorbs by using the climbing nudged elastic band method (CI-NEB) [21].

3.3.3 Verify the transition state structure through the vibrational frequency

3.3.4 Discuss the activation energy results of the coke diffusion from the most stable active site to other stable active sites of each catalyst surfaces.

### 3.4 Rate of coke diffusion

3.4.1. Separate the stage of coke reaction to 3 stages such as the initial stage, intermediate stage, and the final stage

3.4.2 Calculate rate constant ( $k_i$ ) follows the equation:

$$k_i = \frac{k_B T}{h} \exp\left(\frac{-\Delta G_i}{k_B T}\right) \quad (30)$$

Where  $h$  is the Planck's constant equal to  $4.14 \times 10^{-15} \text{ eV s}^{-1}$  and  $k_B$  is the Boltzmann constant, which equals to  $8.617 \times 10^{-5} \text{ eV K}^{-1}$ . In this work, the temperature ( $T$ ) was operated at 1000 K The  $\Delta G_i$  is standard molar Gibbs free energy changes from the initial state to transition state. was calculated by

$$\Delta G_i = E_{\text{DFT}} + E_{\text{ZPE}} - RT \ln Q_{\text{vib}} \quad (31)$$

where  $E_{DFT}$  is the total energy of species  $i$  provided from a normal DFT calculation,  $R$  is the gas constant  $1.43 \times 10^{-28} \text{ eV K}^{-1} \text{ mol}^{-1}$ ,  $Q_{vib}$  is the total vibrational partition function of the adsorbed system in which the measurement from vibrational analysis and  $E_{ZPE}$  is the zero-point energy of the adsorbed system given by

$$\Delta E_{ZPE} = \sum \frac{h\nu_i}{2} \quad (32)$$

Where  $\nu_i$  is the vibrational frequency obtained via the vibrational frequency calculation, and  $h$  is the Planck's constant.

The total vibrational partition function ( $Q_{vib}$ ) was calculated following equation:

$$Q_{vib} = \prod_1^n \frac{1}{(1 - e^{-h\nu_i/K_B T})} \quad (33)$$

The rate of carbon diffusion was operated at temperature 1000 K and calculated via the Matlab software through the following equation:

$$\bar{r} = f_1 \hat{r}_1 + f_2 \hat{r}_2 + f_3 \hat{r}_3 \quad (34)$$

Where  $\bar{r}$  is the total rate of carbon diffusion,  $f_i$  is the surface fraction of each metal and  $\hat{r}_i$  is the rate of carbon diffusion of each pure catalyst.

$$\hat{r} = k_f \theta_{start} - k_r \theta_{end} \quad (35)$$

Where  $k_f$  is the forward rate constant of carbon diffusion,  $k_r$  is the reverse rate constant of carbon diffusion,  $\theta_{start}$  represent surface coverage of the most stable active site that carbon adsorbs on the catalyst surface, and  $\theta_{end}$  represent surface coverage of the active site with the easiest way that carbon from  $\theta_{start}$  diffuse to adsorb.

## CHAPTER IV

### RESULTS AND DISCUSSION

The DFT calculations were performed via the Vienna Ab initio simulation package (VASP) based on the projector augmented wave (PAW). The exchange-correlation function, along with the generalized gradient approximation (GGA) by Perdew, Burke, and Ernzerhof (PBE), were used. The cutoff energy of 300 eV, energy convergence of  $1.0 \times 10^{-6}$  eV/atom force convergence of 0.05 eV/Å, the 3x3x1 Monkhorst-Pack grid k-mesh of 3x3x1 were used to construct the Brillouin-zone integration were used, and the Van der Waals dispersion is described with the DFT-D3 method proposed by Grimme et al. was used.

#### 4.1 Bulk optimization

Before doing every calculation. There were many parameters, whether it be cutoff energy (ENCUT), KPOINTS, and so on, that must be checked to confirm the accuracy of calculations.

The Ni surface model was made from Material Studio. Because the radius and lattice constant of Ni and Co were similar [22, 23], the NiCo bimetallic surfaces were modelled by adding Co into Ni surface and instead some Ni atom with Co atom base on well-dispersion of Co on Ni surface. The results of the bulk optimization, as shown in figure 4. For ENCUT optimization, from the graph (a), which was plotted between ENCUT versus total energy showing the energy start stables at ENCUT 300 – 400 eV, which for real calculation. However, using a higher ENCUT showed better accuracy, a lower ENCUT take a shorter time. When ENCUT reached 400 eV, the total energy did not significantly change when compared with the total energy with 300 eV. Because of the scarcity of resources, therefore, ENCUT 300 eV was used in this

calculation. For KPOINTS optimization, the energy started stables at KPOINTS 5x5x1 and with the same reason for choosing ENCUT; thus, KPOINTS was changed to use 3x3x1 instead.

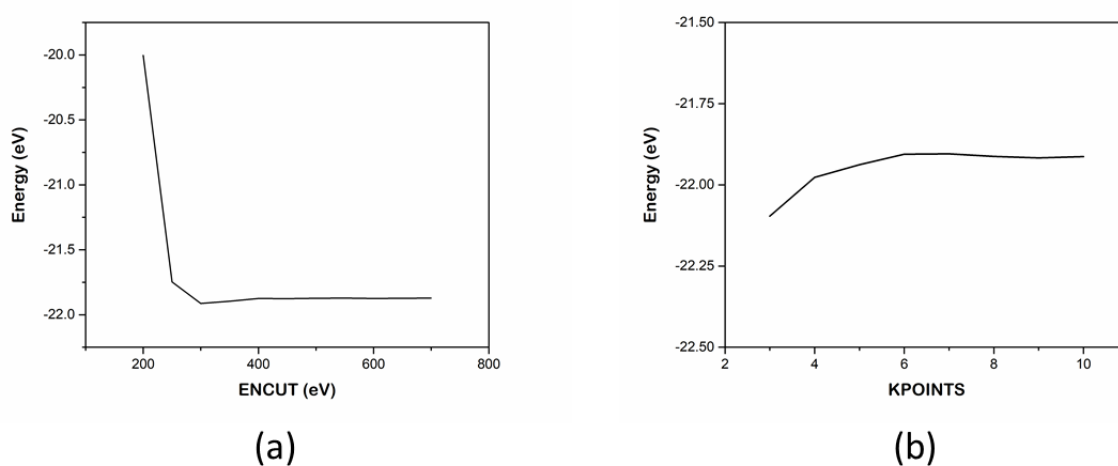


Figure 4 ENCUT and KPOINTS convergence test

## 4.2 Structure optimization

All structure models consisted of a 10-Å-vacuum-region along the z-axis to avoid interactions from the periodicity. The 100 and 111 surfaces of Ni and NiCo catalysts provided five surfaces, and surface 211 provided three surfaces. The fifth layer of 100 and 111 surfaces represented their top layer and the third layer of 211 surface represented its top layer. There were two top layers which were fully relaxed for surface 100 and 111, and only the top layer for surface 211, and the others were fixed. The structure of Ni and NiCo was shown in Figure 5. All possible active sites on the Ni(100), Ni(111), and Ni(211) were shown in Figure 6.



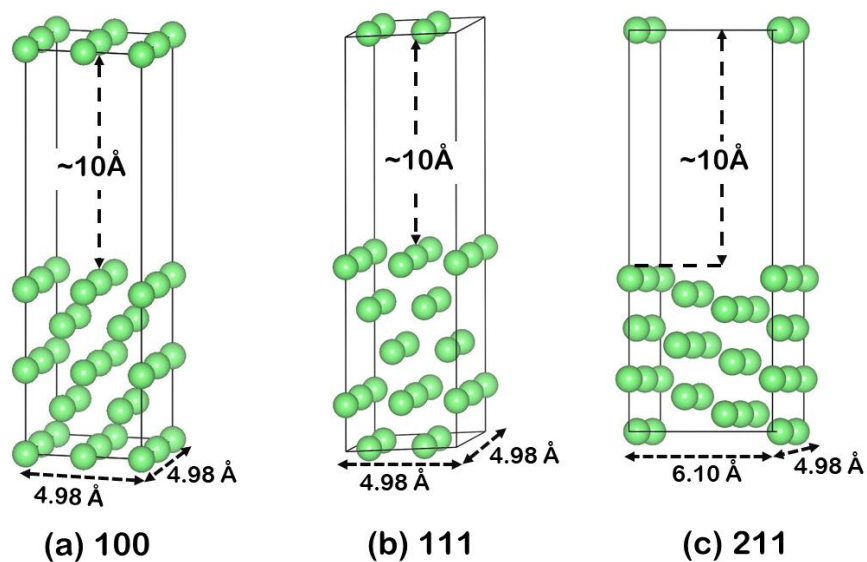


Figure 5 structure of surface (a) 100, (b) 111, and (c) 211 models

All possible active sites are (1) Atop Ni, (2) Atop Co, (3) Bridge Ni-Ni, (4) Bridge Co-Co, (5) Bridge Ni-Co, (6) Fcc (Ni<sub>3</sub>), (7) Fcc (Ni<sub>2</sub>-Co<sub>1</sub>), (8) Fcc (Ni<sub>1</sub>-Co<sub>2</sub>), (9) Hcp (Ni<sub>3</sub>), (10) Hcp (Ni<sub>2</sub>-Co<sub>1</sub>), (11) Hcp (Ni<sub>1</sub>-Co<sub>2</sub>), (12) 4Fold (Ni<sub>4</sub>), (13) 4Fold (Ni<sub>2</sub>-Co<sub>2</sub>), (14) 3Fold (Ni<sub>3</sub>), (15) 3Fold (Ni<sub>2</sub>-Co<sub>1</sub>), (16) 3Fold (Ni<sub>1</sub>-Co<sub>2</sub>), (17) Hcp (Co<sub>3</sub>), and (18) 3Fold (Co<sub>3</sub>).

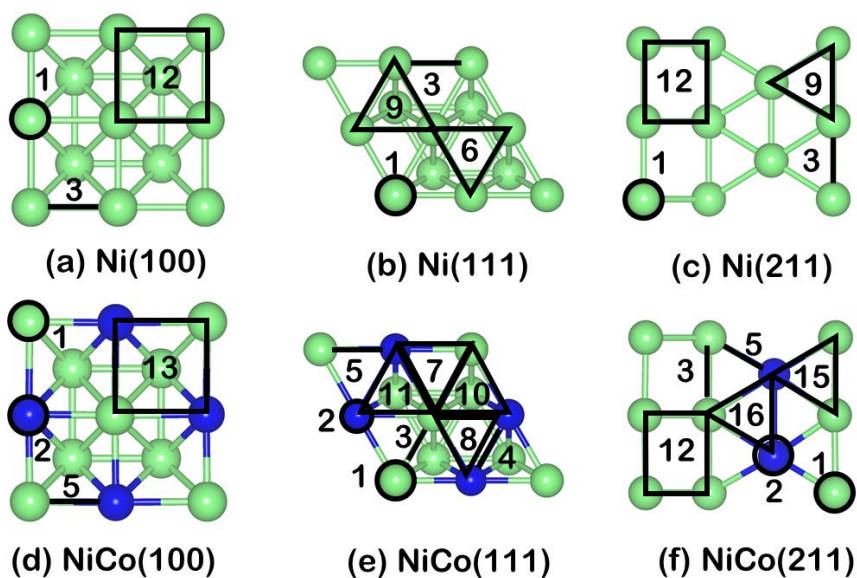


Figure 6 Possible active sites of (a) Ni(100), (b) Ni(111), (c) Ni(211), (d) NiCo(100), (e) NiCo(111), and (f) NiCo(211) surfaces catalysts.

### 4.3 Coke adsorption on the catalyst surface

Coke adsorption or coke formation on catalyst surface was a part of the investigation of catalyst stability. In this part, the ability of coke adsorption was examined through adsorption energy ( $E_{ads}$ ). The negative value of  $E_{ads}$  characterizes attractive interaction between carbon and catalyst surface, and the lower  $E_{ads}$  value represents the stronger interaction of them. The higher  $E_{ads}$  value represented a higher coke resistance.

For each catalyst surface, as shown in Table 6, there were many different possible active sites. It also showed the adsorption sites or the stable active sites, which were optimized since some active sites were not stable active sites for carbon adsorption. This part exhibited a stable active site, which represented the active site that carbon can adsorb on it. The stable active site with the lowest  $E_{ads}$  value of each catalyst surface was used to be the representative active site of each surface. The most stable configuration of 1<sup>st</sup>, 2<sup>nd</sup>, and 3<sup>rd</sup> carbon adsorption on each catalyst surfaces was shown in Figure 7, 8, and 9 respectively. The stable active site with the lowest  $E_{ads}$  value referred to the most attractive site or the most stable active site for adsorption that made it was the first site that carbon should choose to adsorb.

Table 6 The possible active sites and adsorption sites of 1<sup>st</sup> carbon adsorption on Ni(100), Ni(111), Ni(211), NiCo(100), NiCo(111), and NiCo(211) catalysts.

Catalyst surface	1 <sup>st</sup> Carbon adsorption	
	Possible active site	Stable active site
Ni(100)	4Fold	4Fold
	Bridge	4Fold
	Atop	4Fold
Ni(111)	Hcp	Hcp
	Fcc	Fcc
	Atop	Hcp
	Bridge	Hcp

Catalyst surface	1 <sup>st</sup> Carbon adsorption	
	Possible active site	Stable active site
Ni(211)	3Fold	3Fold
	4Fold	4Fold
	Atop	3Fold
	Bridge	3Fold
NiCo(100)	4Fold (Ni <sub>2</sub> -Co <sub>2</sub> )	4Fold (Ni <sub>2</sub> -Co <sub>2</sub> )
	Atop Ni	4Fold (Ni <sub>2</sub> -Co <sub>2</sub> )
	Atop Co	4Fold (Ni <sub>2</sub> -Co <sub>2</sub> )
	Bridge (Ni-Co)	4Fold (Ni <sub>2</sub> -Co <sub>2</sub> )
NiCo(111)	Fcc (Ni <sub>1</sub> -Co <sub>2</sub> )	Fcc (Ni <sub>1</sub> -Co <sub>2</sub> )
	Fcc (Ni <sub>2</sub> -Co <sub>1</sub> )	Fcc (Ni <sub>2</sub> -Co <sub>1</sub> )
	Hcp (Ni <sub>1</sub> -Co <sub>2</sub> )	Hcp (Ni <sub>1</sub> -Co <sub>2</sub> )
	Hcp (Ni <sub>2</sub> -Co <sub>1</sub> )	Hcp (Ni <sub>2</sub> -Co <sub>1</sub> )
	Atop Ni	Fcc (Ni <sub>2</sub> -Co <sub>1</sub> )
	Atop Co	Hcp (Ni <sub>2</sub> -Co <sub>1</sub> )
	Bridge (Ni-Ni)	Fcc (Ni <sub>2</sub> -Co <sub>1</sub> )
	Bridge (Co-Co)	Hcp (Ni <sub>1</sub> -Co <sub>2</sub> )
	Bridge (Ni-Co)	Hcp (Ni <sub>2</sub> -Co <sub>1</sub> )
NiCo(211)	4Fold (Ni <sub>4</sub> )	4Fold (Ni <sub>4</sub> )
	3Fold (Ni <sub>1</sub> -Co <sub>2</sub> )	3Fold (Ni <sub>1</sub> -Co <sub>2</sub> )
	3Fold (Ni <sub>2</sub> -Co <sub>1</sub> )	3Fold (Ni <sub>2</sub> -Co <sub>1</sub> )
	Atop Ni	4Fold (Ni <sub>4</sub> )
	Atop Co	3Fold (Ni <sub>2</sub> -Co <sub>1</sub> )
	Bridge (Ni-Ni)	3Fold (Ni <sub>2</sub> -Co <sub>1</sub> )
	Bridge (Co-Co)	3Fold (Ni <sub>1</sub> -Co <sub>2</sub> )

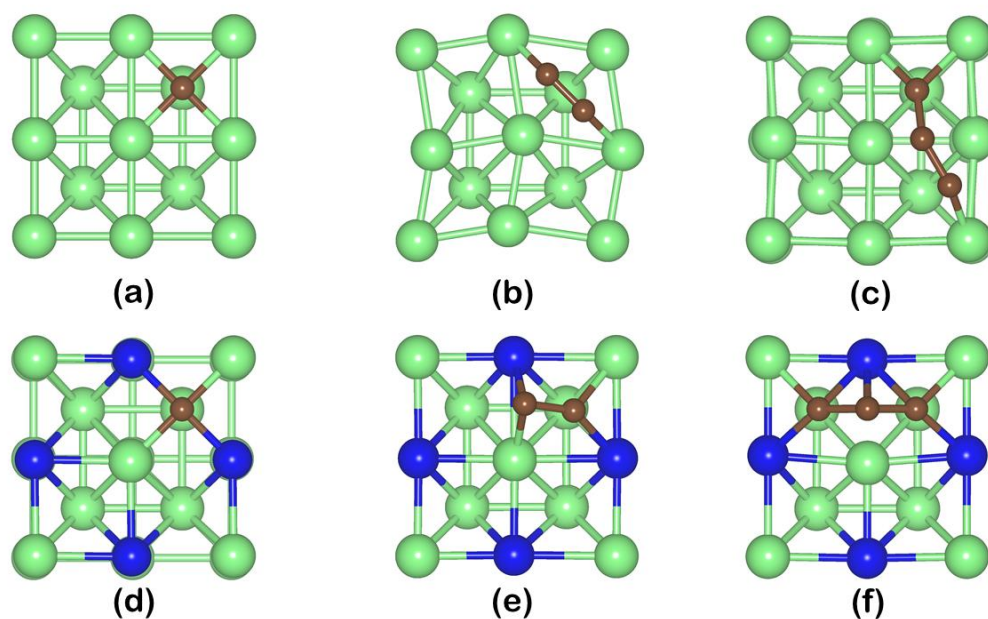


Figure 7 The most stable configuration of 1<sup>st</sup>, 2<sup>nd</sup>, and 3<sup>rd</sup> coke adsorption on (a-c) Ni(100) and (d-f) NiCo(100)

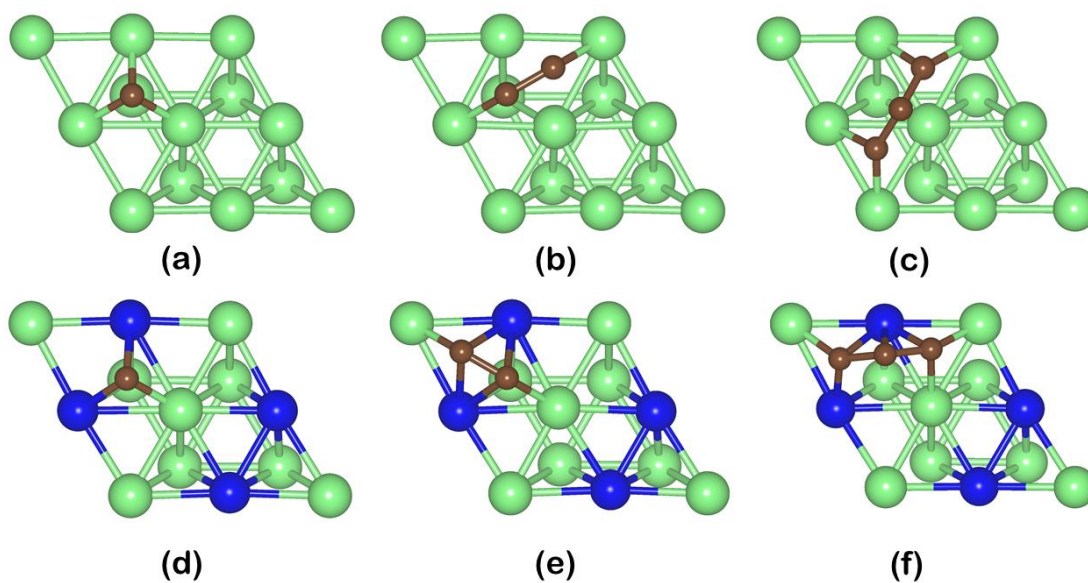


Figure 8 The most stable configuration of 1<sup>st</sup>, 2<sup>nd</sup>, and 3<sup>rd</sup> coke adsorption on (a-c) Ni(111) and (d-f) NiCo(111)

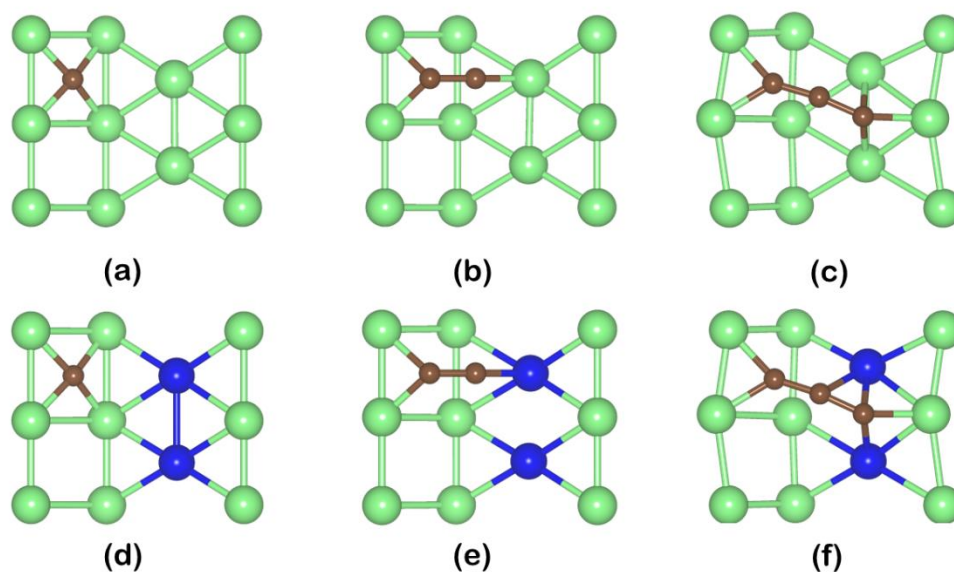


Figure 9 The most stable configuration of of 1<sup>st</sup>, 2<sup>nd</sup>, and 3<sup>rd</sup> coke adsorption on (a-c) Ni(211) and (d-f) NiCo(211)

As the results in Table 7, The Eads of the first carbon adsorption of NiCo catalyst in all surface such as 100, 111 and 211 exhibited a weaker adsorption strength than Ni catalyst. Almost all surfaces of NiCo catalyst, as shown in Table 8, exhibited higher Eads of second and third coke adsorption, which meant the NiCo catalyst was more performance of coke resistance than Ni catalyst. The surface 111 of both catalysts showed the best ability of coke resistance that investigated from the lowest Eads value out of all surfaces. The coke adsorption energies of a noble metal catalyst such as Pd, Rh, Ru were calculated with the same condition of Ni and NiCo catalyst. As the results from Table 9, Some surfaces of NiCo catalyst showed the Eads value approximate to the noble catalyst, and some surfaces of NiCo showed higher coke adsorption energies value than noble catalyst surface. It may be approximately concluded that adding Co into Ni to form NiCo catalyst contributed a performance of coke preventing could be comparable with or better than the noble catalyst. Ni and NiCo catalyst bound by surface 111 exhibited the best coke resistance performance. The adsorption energy correlated with the equilibrium

adsorption height ( $d_{c-sur}$ ) as shown in Table 10. The lower  $d_{c-sur}$  resulted in stronger interaction between coke and catalyst surface. Both Ni and NiCo catalyst, surface 111 showed highest  $d_{c-sur}$  which involved with the adsorption energy that surface 111 exhibited the weakest interaction between coke and catalyst surface.

Table 7 Adsorption energies of 1<sup>st</sup> carbon adsorption on adsorption sites of Ni(100), Ni(111), Ni(211), NiCo(100), NiCo(111), and NiCo(211) catalysts.

Catalyst surface	1 <sup>st</sup> Carbon adsorption	
	Adsorption site	Adsorption energy (eV)
Ni(100)	4Fold	-8.34
Ni(111)	Hcp	-6.99
	Fcc	-6.88
Ni(211)	3Fold	-6.85
	4Fold	-7.94
NiCo(100)	4Fold (Ni2-Co2)	-8.22
NiCo(111)	Fcc (Ni1-Co2)	-6.84
	Fcc (Ni2-Co1)	-6.79
	Hcp (Ni1-Co2)	-7.00
	Hcp (Ni2-Co1)	-6.92
NiCo(211)	4Fold (Ni4)	-7.69
	3Fold (Ni1-Co2)	-6.87
	3Fold (Ni2-Co1)	-6.94

Table 8 Adsorption energies of 1<sup>st</sup>, 2<sup>nd</sup>, and 3<sup>rd</sup> carbon adsorption on Ni(100), Ni(111), Ni(211), NiCo(100), NiCo(111), and NiCo(211) surfaces catalysts.

Catalyst surface	Adsorption energy (eV)		
	1 <sup>st</sup> Carbon	2 <sup>nd</sup> Carbon	3 <sup>rd</sup> carbon
Ni(100)	-8.34	-7.63	-6.96
Ni(111)	-6.99	-7.26	-6.00
Ni(211)	-7.94	-8.28	-7.62
NiCo(100)	-8.22	-7.42	-7.40
NiCo(111)	-7.00	-7.33	-5.92
NiCo(211)	-7.69	-8.20	-7.43

Table 9 Adsorption energies of 1<sup>st</sup>, 2<sup>nd</sup>, and 3<sup>rd</sup> carbon adsorption on Ni(100), Ni(111), Ni(211), NiCo(100), NiCo(111), and NiCo(211) surfaces catalysts.

Catalyst surface	Adsorption energy (eV)		
	1 <sup>st</sup> Carbon	2 <sup>nd</sup> Carbon	3 <sup>rd</sup> Carbon
Pd(100)	-8.09	-7.13	-6.05
Pd(111)	-7.40	-6.82	-6.01
Pd(211)	-8.07	-8.02	-6.97
Rh(100)	-8.42	-8.11	-7.32
Rh(111)	-7.62	-7.52	-6.73
Rh(211)	-8.10	-8.49	-7.55

Table 10 Equilibrium adsorption height ( $d_{c-sur}$ ) of 1<sup>st</sup> carbon adsorption on Ni(100), Ni(111), Ni(211), NiCo(100), NiCo(111), and NiCo(211) surfaces catalysts.

Catalyst surface	Equilibrium adsorption height ( $d_{c-sur}$ ) (Å)
Ni(100)	0.28
Ni(111)	0.97
Ni(211)	0.25
NiCo(100)	0.32
NiCo(111)	0.95
NiCo(211)	0.26

#### 4.4 Adsorption properties of catalyst surfaces

According to Hammer and Nørskov model, the d-band center can be used to indicate the adsorption properties of clean metal surfaces. The d-band center, which was lower or closer to the Fermi level referred to the stronger bond or greater the interaction between adsorbate and adsorbent [24]. It could be concluded that a higher d-band center or closer to the Fermi level results in stronger bonding and likewise, a lower d-band center or the farther means weaker bonding.

From the  $\epsilon_d$  value results, as shown in Table 11, on the clean surface, the  $\epsilon_d$  value of Ni on the top surface of NiCo bimetallic catalyst was lower than Ni on the top surface of Ni catalyst. It means NiCo showed a weaker bonding between the adsorbate referring to a carbon atom and the adsorbent referring to the catalyst surface. Although the  $\epsilon_d$  value of Co was low when it was the Co monometallic, Co showed the high  $\epsilon_d$  value when it was the NiCo bimetallic. As the results of NiCo catalyst surface, Co exhibited the closer  $\epsilon_d$  value than Ni that mean Co showed



stronger bonding with coke than Ni. Adding Co could decrease the  $\epsilon_d$  value of Ni in NiCo bimetallic catalyst.

The  $\epsilon_d$  value of NiCo bimetallic catalyst and Ni monometallic catalyst that was adsorbed with carbon atom were compared. Almost all NiCo bimetallic surfaces exhibited the lower  $\epsilon_d$  value than Ni monometallic surfaces which mean adding Co on NiCo bimetallic catalyst contributed the destabilization of the Ni-coke interaction that lead to increase the stability of the catalyst. The surface 111 of NiCo and Ni exhibited the lowest  $\epsilon_d$  value out of their all surfaces, which meant surface 111 showed the weakest bonding between coke and catalyst surface referring to the best performance of coke resistance.

Table 11 The d-band center ( $\epsilon_d$ ) at the top surface for Ni and Co on Ni, Co monometallic and NiCo bimetallic catalyst.

Catalyst	Carbon atom	$\epsilon_d$ (eV)		
		Ni	Co	NiCo
NiCo(100)	Clean surface	-1.30	-1.31	-1.31
	1	-1.32	-1.12	-1.22
	2	-1.42	-1.27	-1.35
	3	-1.61	-1.25	-1.43
NiCo(111)	Clean surface	-1.38	-1.30	-1.34
	1	-1.35	-1.20	-1.28
	2	-1.40	-1.24	-1.32
	3	-1.69	-1.34	-1.52
NiCo(211)	Clean surface	-1.37	-1.42	-1.40
	1	-1.52	-1.31	-1.42
	2	-1.43	-1.33	-1.38
	3	-1.48	-1.42	-1.45

Ni(100)	Clean surface	-1.13	-	-
	1	-1.25	-	-
	2	-1.31	-	-
	3	-1.42	-	-
Ni(111)	Clean surface	-1.12	-	-
	1	-1.50	-	-
	2	-1.44	-	-
	3	-1.51	-	-
Ni(211)	Clean surface	-1.31	-	-
	1	-1.26	-	-
	2	-1.34	-	-
	3	-1.39	-	-
Co(001)	Clean surface	-	-1.25	-
	1	-	-1.52	-
	2	-	-1.34	-
	3	-	-1.55	-

#### 4.5 Coke movement on the catalyst surface

The stability assessment apart from the ability of coke resistance, there was also the ability of coke movement on the catalyst surface, which could be evaluated through the activation energy ( $E_a$ ) or energy barrier of coke movement on the catalyst surface. Easier coke movement leads to getting more chances to against another atom such as O, H, and C atom that lower activation energy means more chances for binding. In this part, we calculate  $E_a$  of coke diffusing from the most stable active site and adsorb on another stable active site. In the first step, coke started to adsorb on the most stable active site because it was the most attractive site. The next step was a coke movement or coke diffusion from the most stable active site and adsorb on another stable active site. The coke diffusion represented the ability of coke removal because if the catalyst surface can easily diffuse coke

from the surface that meant it easily remove coke from the surface. The activation energy was the minimum energy required to cause a process or chemical reaction to occur since the carbon started diffusing when it got enough energy, which was equal to or higher than  $E_a$  of diffusion. Lower activation energy referred to easier the occurrence of the chemical reaction. Similarly, A higher activation energy means more difficult the occurrence of the chemical reaction.

The results of the activation energy of the coke movement were shown in Table 12. The Ni(100) and NiCo(100) surfaces had only one stable active site that referred to carbon will adsorb on only one active, or there are no other stable active sites for carbon adsorption since it could be referred to there is no coke movement on Ni(100) and NiCo(100) surfaces.

For Ni(111), NiCo(111), Ni(211), and NiCo(211) surfaces, there are stable active sites with more than one active site, which means there is a coke movement on catalyst surfaces. In this part, the coke movement pathway with the lowest  $E_a$  value was investigated for the reason that it was the easiest pathway and should be the first pathway for coke movement or coke diffusion. Both Ni and NiCo catalysts exhibited lower  $E_a$  value of surface 111 than surface 211 that meant surface 111 exhibited higher performance of the coke movement more than surface 211. All surfaces of NiCo catalyst showed the lower  $E_a$ s than Ni catalyst when compared with the identical surface which means NiCo catalyst was the catalyst which showed better performance of coke movement than Ni catalyst and may be approximately concluded NiCo catalyst was a catalyst which exhibited better performance of coke removal from the catalyst surface or higher stability.

Table 12 The activation energies for the forward ( $E_{a,f}$ ) and reverse ( $E_{a,r}$ ) for coke movement reaction on Ni(100), Ni(111), Ni(211), NiCo(100), NiCo(111), and NiCo(211) surfaces catalysts.

Catalysts	Surface	Elementary step	$E_{a,f}$ (eV)	$E_{a,r}$ (eV)
Ni	111	$C_{Hcp} \rightarrow C_{Fcc}$	0.50	0.39
	211	$C_{4Fold} \rightarrow C_{3Fold}$	1.42	0.34
Ni-Co	111	$C_{HcpNi1} \rightarrow C_{FccNi1}$	0.34	0.19
	211	$C_{4Fold} \rightarrow C_{3FoldNi2}$	1.01	0.26
Co	001	$C_{HCP} \rightarrow C_{3Fold}$	0.42	0.19

#### 4.6 Rate of coke diffusion

The coke diffusion was represented the ability of coke removal because if the catalyst surface can easily diffuse coke on the surface that meant it easily remove coke from the surface. The high rate of coke diffusion referred to high stability. For this research, coke diffusion was the coke movement from the most stable active site ( $\theta_{start}$ ) to another stable active site ( $\theta_{end}$ ). Although there are many pathways of coke movement, in this work, the easiest pathway or the pathway with the lowest  $E_a$  value was investigated because it was the first pathway of coke diffusion or coke movement. In this part, The NiCo bimetallic catalyst was implied that it did not contain only the content of NiCo bimetallic. Conversely, it contained the content of Ni, Co monometallic, and the content of NiCo bimetallic, as shown in Figure 11. The representative stable active site of NiCo, Ni, and Co catalysts was

NiCo(111), Ni(111), and Co(001) surfaces. The coke adsorption providing into 3 steps represented each time period of reaction such as the beginning step, the intermediate step, and the final step, as shown in Figure 10.

The beginning step was the step at the first time of reaction. In this step, the catalyst surface was clean or had no coke on the catalyst surface. The coke should firstly adsorb on the most stable active site because it is the most favorable active site. The results, as shown in Figure 10(a), exhibited an increase of NiCo bimetallic content will increase the rate of coke diffusion will be high. In contrast, the increase in the content of Co monometallic will decrease the rate of coke diffusion. Moreover, the content of Ni monometallic almost did not affect the rate of coke diffusion. For the reason that the beginning step, coke should firstly adsorb on the most stable active site, so  $\theta_{\text{start}}$  equal to 0.1 and  $\theta_{\text{end}}$  equal to 0.0.

After the first stable active site was fully adsorbed with coke. The coke will adsorb on another active site, which is the second most stable active site. In this step, was next beginning step represented the intermediate step, as shown in Figure 10(b). As a result, when increased the NiCo bimetallic content, the rate of coke diffusion was still high. However, the effect of Co content on the rate of coke diffusion decreased from the beginning step, and the content of Ni monometallic still almost did not affect the rate of coke diffusion.

The final step represented the catalyst surface, which was fully covered with coke. From the results, as shown in Figure 10(c), Almost all of the catalyst surface showed no rate of coke diffusion for a reason that on the catalyst surface fully covered with coke resulting in there is no place for coke adsorption. Every surface and all catalyst content almost did not affect the rate of coke diffusion.

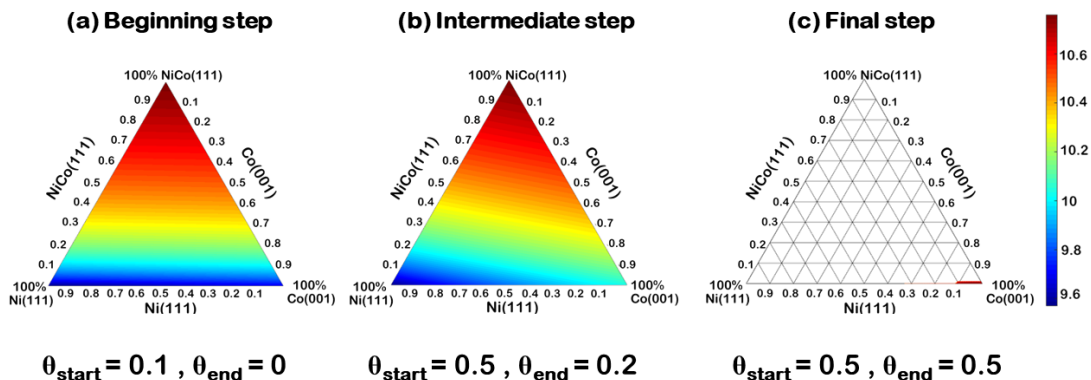


Figure 10 The total rate of coke diffusion under 1000 K at (a) beginning step, (b) intermediate step, and (c) final step.

#### 4.7 Design and guideline of catalyst

The NiCo bimetallic catalyst model for this research was designed. In a bimetallic catalyst did not contain only NiCo bimetallic content. However, it contained Ni monometallic, Co monometallic, and NiCo bimetallic, as shown in Figure 11.

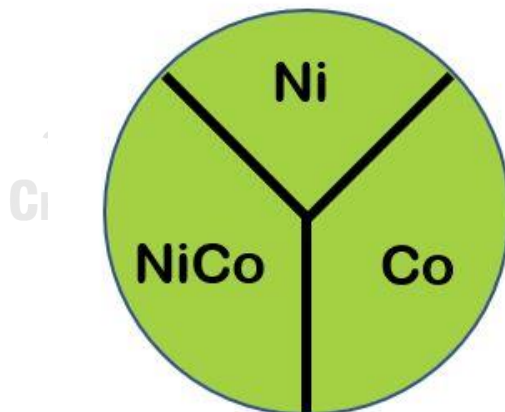


Figure 11 the NiCo bimetallic model

From the results, as shown in Figure 10, the NiCo bimetallic catalyst reached a high coke diffusion rate when it contained a high content of the NiCo surface.

However, for use in the industrial, many factors have to be considered, such as activity and selectivity.

From the results, as shown in Figure 10, the content of NiCo bimetallic mostly affect the rate of coke diffusion for the NiCo bimetallic catalyst. In contrast, the Co monometallic content exhibited a negative effect on the improvement rate of coke diffusion on the NiCo bimetallic catalyst and the Ni monometallic content exhibited almost no contribution to the improvement rate of coke diffusion

The NiCo bimetallic containing with the high content of NiCo bimetallic. It will exhibit a high rate of coke diffusion, which meant the high performance of coke removal on the catalyst surface. For this reason, NiCo bimetallic catalyst should including low content of Ni and Co monometallic.

Adding Co can improve the stability of NiCo bimetallic catalysts such as reducing the coke adsorption energy on the catalyst surface, which meant improve the ability of coke resistance and reducing the activation energy of coke diffusion, which means improve the ability of coke removal.

## CHAPTER v

### CONCLUSION

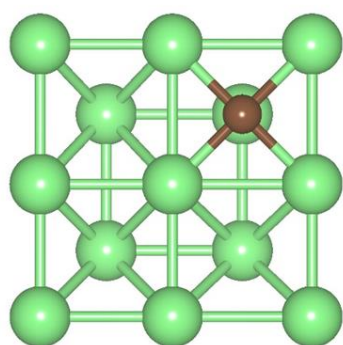
The stability assessment for dry reforming of methane reaction was investigated through 2 main factors are the performance of coke resistance and the ability of coke removal. For the performance of coke, resistance was considered through the coke adsorption energy on the catalyst surface, Ni catalyst was a catalyst exhibiting the comparable activity to noble catalysts such as Rh, Ru, and Pd. However, it exhibited a terrible performance of coke resistance. Adding Co into Ni catalyst forming the NiCo bimetallic catalyst was an alternative way to improve the performance of coke resistance. The NiCo bimetallic catalyst exhibited better performance of coke resistance than Ni catalysts, and it also could be comparable or better than noble catalysts. The stability assessment was also considered through the ability of coke removal, which was considered through the activation energy of the coke movement on catalyst surface or coke diffusion from the most stable active to another stable active site. Both Ni and NiCo catalysts were not considered surface 100 because there was only one stable active site referring to there was no coke movement on its surface. They also exhibited the lowest and highest activation energy on surface 111 and 211 respective. NiCo catalyst exhibited a higher ability of coke removal than Ni catalysts from comparing the activation energy of the coke movement with an identical surface. The part of NiCo catalyst was dividing into 3 parts were (1) Ni monometallic, (2) Co monometallic, and (3) NiCo bimetallic. In order to get a high rate of coke diffusion, the NiCo catalyst must contain a high content of NiCo bimetallic and low content of Ni and Co monometallic.



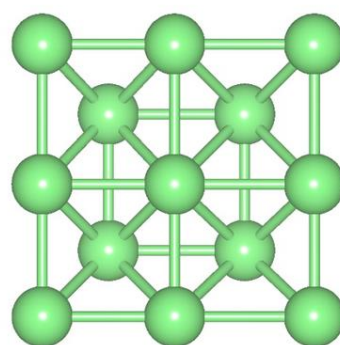


APPENDIX A  
CALCULATION FOR ADSORPTION ENERGY

For example, carbon adsorption on 4fold site of Ni(111) catalyst.



$$E_{\text{complex}} = -118.22 \text{ eV}$$



$$E_{\text{surface}} = -108.54 \text{ eV}$$

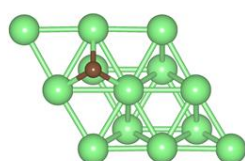


$$E_{\text{coke}} = -1.34 \text{ eV}$$

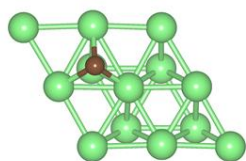
$$\begin{aligned} E_{\text{ads}} &= E_{\text{complex}} - (E_{\text{coke}} + E_{\text{surface}}) \\ &= -118.22 - ((-108.54) + (-1.34)) \\ &= -8.34 \text{ eV} \end{aligned}$$

APPENDIX B  
CALCULATION FOR ADSORPTION ENERGY

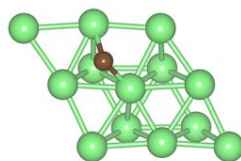
For example, carbon on Ni(111) surface move from Hcp site to Fcc site



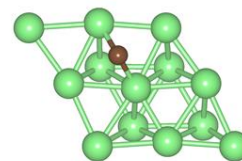
$$E_0 = -118.75 \text{ eV}$$



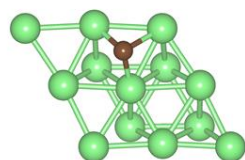
$$E_1 = -118.73 \text{ eV}$$



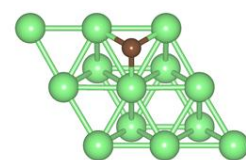
$$E_2 = -118.50 \text{ eV}$$



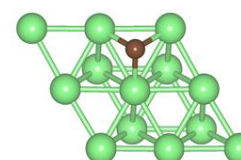
$$E_3 = -118.25 \text{ eV}$$



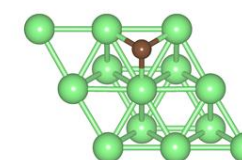
$$E_4 = -118.52 \text{ eV}$$



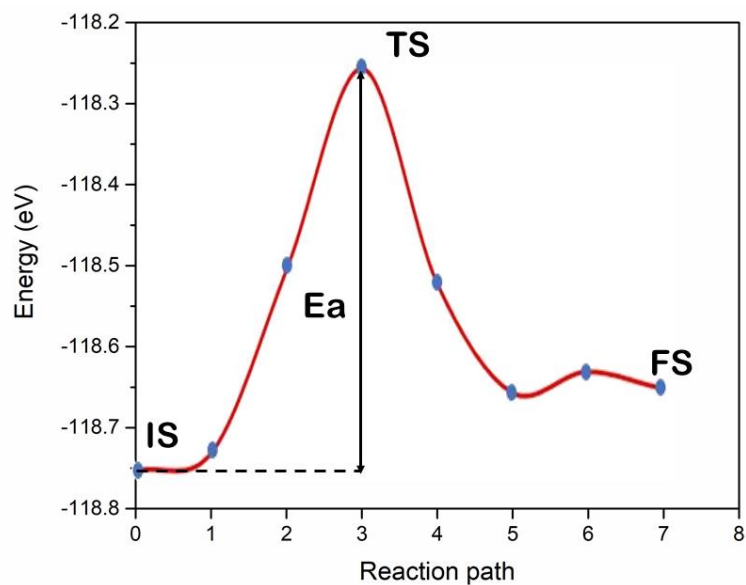
$$E_5 = -118.66 \text{ eV}$$



$$E_6 = -118.63 \text{ eV}$$



$$E_7 = -118.65 \text{ eV}$$



$$E_{IS} = -118.75 \text{ eV} , E_{TS} = E_3 = -118.25$$

$$E_a = E_{TS} - E_{IS} = (-118.25) - (-118.75)$$

$$= 0.5 \text{ eV}$$

## APPENDIX C

## CALCULATON FOR RATE OF COKE DIFFUSION

For example, Carbon diffusion on Ni(111) surface from Hcp site to Fcc site

Table 13 Vibrational frequency of Initial state (Hcp)

$\nu$ (cm <sup>-1</sup> )	$\nu$ (s <sup>-1</sup> )	qvib	E <sub>ZPE</sub> (eV)
667.399	2.00×10 <sup>13</sup>	1.620	0.0414
613.399	1.84×10 <sup>13</sup>	1.705	0.0381
612.051	1.84×10 <sup>13</sup>	1.707	0.0380
270.701	8.12×10 <sup>12</sup>	3.098	0.0168
270.277	8.11×10 <sup>12</sup>	3.102	0.0168
269.905	8.10×10 <sup>12</sup>	3.106	0.0167
268.156	8.04×10 <sup>12</sup>	3.122	0.0166
261.642	7.85×10 <sup>12</sup>	3.186	0.0162
260.875	7.83×10 <sup>12</sup>	3.194	0.0162
247.879	7.44×10 <sup>12</sup>	3.332	0.0154
217.716	6.53×10 <sup>12</sup>	3.716	0.0135
217.141	6.51×10 <sup>12</sup>	3.725	0.0135
214.777	6.44×10 <sup>12</sup>	3.760	0.0133
184.895	5.55×10 <sup>12</sup>	4.279	0.0115
178.721	5.36×10 <sup>12</sup>	4.408	0.0111
177.720	5.33×10 <sup>12</sup>	4.429	0.0110
149.117	4.47×10 <sup>12</sup>	5.176	0.0093
147.732	4.43×10 <sup>12</sup>	5.219	0.0092
146.663	4.40×10 <sup>12</sup>	5.253	0.0091
146.470	4.39×10 <sup>12</sup>	5.260	0.0091
140.359	4.21×10 <sup>12</sup>	5.465	0.0087
137.957	4.14×10 <sup>12</sup>	5.551	0.0086
103.227	3.10×10 <sup>12</sup>	7.241	0.0064

100.313	$3.01 \times 10^{12}$	7.436	0.0062
97.435	$2.92 \times 10^{12}$	7.640	0.0060
36.228	$1.09 \times 10^{12}$	19.676	0.0022
33.111	$9.93 \times 10^{11}$	21.481	0.0021

Table 14 Vibrational frequency of transition state

$\nu$ (cm <sup>-1</sup> )	$\nu$ (s <sup>-1</sup> )	qvib	E <sub>ZPE</sub> (eV)
775.265	$2.33 \times 10^{13}$	1.487	0.0481
701.087	$2.10 \times 10^{13}$	1.573	0.0435
291.550	$8.75 \times 10^{12}$	2.917	0.0181
280.306	$8.41 \times 10^{12}$	3.011	0.0174
275.122	$8.25 \times 10^{12}$	3.057	0.0171
269.207	$8.08 \times 10^{12}$	3.112	0.0167
260.672	$7.82 \times 10^{12}$	3.196	0.0162
255.531	$7.67 \times 10^{12}$	3.249	0.0159
244.150	$7.32 \times 10^{12}$	3.374	0.0151
226.019	$6.78 \times 10^{12}$	3.600	0.0140
215.540	$6.47 \times 10^{12}$	3.748	0.0134
211.204	$6.34 \times 10^{12}$	3.814	0.0131
193.849	$5.82 \times 10^{12}$	4.106	0.0120
187.617	$5.63 \times 10^{12}$	4.224	0.0116
180.448	$5.41 \times 10^{12}$	4.371	0.0112
166.383	$4.99 \times 10^{12}$	4.694	0.0103
161.504	$4.85 \times 10^{12}$	4.820	0.0100
137.877	$4.14 \times 10^{12}$	5.554	0.0086
132.216	$3.97 \times 10^{12}$	5.769	0.0082
127.117	$3.81 \times 10^{12}$	5.979	0.0079
124.597	$3.74 \times 10^{12}$	6.089	0.0077

108.430	$3.25 \times 10^{12}$	6.919	0.0067
97.506	$2.93 \times 10^{12}$	7.635	0.0060
90.491	$2.71 \times 10^{12}$	8.186	0.0056
44.997	$1.35 \times 10^{12}$	15.941	0.0028
30.013	$9.00 \times 10^{11}$	23.645	0.0019
304.510	$9.14 \times 10^{12}$	2.817	0.0189

Table 15 Vibrational frequency of final state (Fcc)

$\nu$ (cm <sup>-1</sup> )	$\nu$ (s <sup>-1</sup> )	qvib	E <sub>ZPE</sub> (eV)
667.152	$2.00 \times 10^{13}$	1.620	0.0414
590.331	$1.77 \times 10^{13}$	1.747	0.0366
588.089	$1.76 \times 10^{13}$	1.751	0.0365
266.253	$7.99 \times 10^{12}$	3.141	0.0165
265.299	$7.96 \times 10^{12}$	3.150	0.0165
264.763	$7.94 \times 10^{12}$	3.155	0.0164
253.214	$7.60 \times 10^{12}$	3.273	0.0157
252.717	$7.58 \times 10^{12}$	3.279	0.0157
247.185	$7.42 \times 10^{12}$	3.339	0.0153
243.293	$7.30 \times 10^{12}$	3.384	0.0151
222.832	$6.68 \times 10^{12}$	3.644	0.0138
211.115	$6.33 \times 10^{12}$	3.815	0.0131
210.843	$6.33 \times 10^{12}$	3.819	0.0131
178.387	$5.35 \times 10^{12}$	4.415	0.0111
177.734	$5.33 \times 10^{12}$	4.429	0.0110
175.539	$5.27 \times 10^{12}$	4.478	0.0109
143.611	$4.31 \times 10^{12}$	5.354	0.0089

143.224	$4.30 \times 10^{12}$	5.367	0.0089
139.452	$4.18 \times 10^{12}$	5.497	0.0087
138.152	$4.14 \times 10^{12}$	5.544	0.0086
136.611	$4.10 \times 10^{12}$	5.601	0.0085
126.758	$3.80 \times 10^{12}$	5.995	0.0079
102.259	$3.07 \times 10^{12}$	7.304	0.0063
97.304	$2.92 \times 10^{12}$	7.650	0.0060
95.039	$2.85 \times 10^{12}$	7.820	0.0059
34.177	$1.03 \times 10^{12}$	20.827	0.0021
31.819	$9.55 \times 10^{11}$	22.332	0.0020

1. Change vibrational frequency ( $\nu$ ) unit from  $\text{cm}^{-1}$  to  $\text{s}^{-1}$  following equation

$$\nu (\text{s}^{-1}) = \nu (\text{cm}^{-1}) \times c (\text{cm/s})$$

where  $c$  is the speed of light equal to  $3 \times 10^{10}$  cm/s

2. Calculate  $q_{\text{vib}}$  following equation

$$q_{\text{vib}} = \frac{1}{(1 - e^{-h\nu/K_B T})}$$

where Planck's constant equal to  $4.14 \times 10^{-15}$  eV  $\text{s}^{-1}$ ,  $k_B$  is the Boltzmann constant equal to  $8.617 \times 10^{-5}$  eV  $\text{K}^{-1}$ ,  $\nu$  is vibrational frequency ( $\text{s}^{-1}$ ) and  $T$  is temperature (K)

3. Calculate the total vibrational partition function ( $Q_{\text{vib}}$ ) following equation

$$Q_{\text{vib}} = \prod_1^n q_{\text{vib}_i}$$

where  $Q_{\text{vib}}$  is the total vibrational partition function of the adsorbed system in which the measurement from vibrational analysis

4. Calculate the zero-point energy ( $E_{ZPE}$ ) following equation

$$\Delta E_{ZPE} = \sum \frac{h\nu_i}{2}$$

Where  $E_{ZPE}$  is the zero-point energy of the adsorbed system

The results from the above calculations were shown in Table 16.

Table 16  $Q_{vib}$  and  $E_{ZPE}$  of the initial state, transition state and final state

Parameter	Initial state	Transition state	Final state
$Q_{vib}$	$2.55 \times 10^{17}$	$1.15 \times 10^{17}$	$5.21 \times 10^{17}$
$E_{ZPE}$ (eV)	0.3829	0.3591	0.3724
Total Energy (eV)	-118.75	-118.25	-118.65

5. Gibbs free energy changes from the initial state to transition state. was calculated by

$$\Delta G_i = E_{DFT} + E_{ZPE} - RT \ln Q_{vib}$$

where  $E_{DFT}$  is the total energy of species  $i$  provided from a normal DFT calculation,  $R$  is the gas constant  $8.62 \times 10^{-5}$  eV  $K^{-1}$ ,  $Q_{vib}$  is the total vibrational partition function of adsorbed system in which the measurement from vibrational analysis and  $E_{ZPE}$  is the zero-point energy of adsorbed system

$\Delta G_i$  can be calculate as above equation:

$$\Delta G_{\text{initial state}} = -118.75 + 0.3829 - (8.62 \times 10^{-5})(1000) \ln(2.55E+17) = -1.22 \times 10^{-2}$$

$$\Delta G_{\text{transition state}} = -118.25 + 0.3591 - (8.62 \times 10^{-5})(1000) \ln(1.15E+17) = -1.21 \times 10^{-2}$$

$$\Delta G_{\text{final state}} = -118.65 + 0.3724 - (8.62 \times 10^{-5})(1000) \ln(5.21E+17) = -1.22 \times 10^{-2}$$



$$\begin{aligned}\Delta G &= \Delta G_{\text{final state}} - \Delta G_{\text{initial state}} = 3.39 \times 10^{-2} \\ \Delta G_{\text{forward}} &= \Delta G_{\text{transition state}} - \Delta G_{\text{initial state}} = 0.546 \\ \Delta G_{\text{reverse}} &= \Delta G_{\text{transition state}} - \Delta G_{\text{final state}} = 0.512\end{aligned}$$

6. Calculate the reaction rate constant ( $k_i$ ) following equation:

$$k_i = \frac{k_B T}{h} \exp\left(\frac{-\Delta G_i}{k_B T}\right)$$

where  $h$  is the Planck's constant equal to  $4.14 \times 10^{-15}$  eV s<sup>-1</sup> and  $k_B$  is the Boltzmann constant equal to  $8.617 \times 10^{-5}$  eV K<sup>-1</sup>. In this work, the temperature ( $T$ ) was operated at 1000 K. The  $\Delta G_i$  is standard molar Gibbs free energy changes from the initial state to transition state, was calculated by

$k_i$  can be calculated as the above equation:

$$\begin{aligned}k_{\text{forward}} &= \frac{(8.617 \times 10^{-5})(1000)}{4.14 \times 10^{-15}} \exp\left(\frac{-0.546}{(8.617 \times 10^{-5})(1000)}\right) = 3.71 \times 10^{-10} \\ k_{\text{reverse}} &= \frac{(8.617 \times 10^{-5})(1000)}{4.14 \times 10^{-15}} \exp\left(\frac{-0.512}{(8.617 \times 10^{-5})(1000)}\right) = 5.49 \times 10^{-10}\end{aligned}$$

7. Calculate the reaction rate ( $\hat{r}_i$ ) following equation:

$$\hat{r} = k_f \theta_{\text{start}} - k_r \theta_{\text{end}}$$

Where  $k_f$  is the forward rate constant of carbon diffusion,  $k_r$  is the reverse rate constant of carbon diffusion,  $\theta_{\text{start}}$  represent surface coverage of the most stable active site that carbon adsorbs on the catalyst surface, and  $\theta_{\text{end}}$  represent surface coverage of the active site with the easiest way that carbon from  $\theta_{\text{start}}$  diffuse to adsorb.

For this research, types of surface coverage were separate to 3 types such as:

1. Beginning step -  $\theta_{\text{start}} \sim 0.1$  and  $\theta_{\text{end}} \sim 0.0$

2. Middle step -  $\theta_{\text{start}} \sim 0.5$  and  $\theta_{\text{end}} \sim 0.2$

3. Final step -  $\theta_{\text{start}} \sim 0.5$  and  $\theta_{\text{end}} \sim 0.5$

Table 17 the results of Forward rate constant and Reverse rate constant of Ni, Co, and NiCo catalyst

Catalyst	$k_{\text{forward}}$	$k_{\text{reverse}}$
Ni	$3.71 \times 10^{-10}$	$5.49 \times 10^{-10}$
Co	$4.88 \times 10^{-10}$	$4.00 \times 10^{-10}$
NiCo	$7.02 \times 10^{-9}$	$2.06 \times 10^{-14}$

$\hat{r}$  of Ni can be calculate as above equation:

$$\hat{r}_1 = \text{rate at beginning step} = (3.71 \times 10^{-10}) (0.1) - (5.49 \times 10^{-10}) (0.0) = 3.71 \times 10^{-11}$$

$$\hat{r}_2 = \text{rate at middle step} = (3.71 \times 10^{-10}) (0.5) - (5.49 \times 10^{-10}) (0.2) = 0.76 \times 10^{-10}$$

$$\hat{r}_3 = \text{rate at final step} = (3.71 \times 10^{-10}) (0.5) - (5.49 \times 10^{-10}) (0.5) = -0.89 \times 10^{-10}$$

For final step rate of coke diffusion is lower than 0 which mean in that time, there is no coke diffusion hence  $\hat{r}_3 = 0$

For example, at the middle step

$$\hat{r}_{\text{Ni}} = (3.71 \times 10^{-10}) (0.5) - (5.49 \times 10^{-10}) (0.2) = 0.76 \times 10^{-10}$$

$$\hat{r}_{\text{Co}} = (4.88 \times 10^{-10}) (0.5) - (4.00 \times 10^{-10}) (0.2) = 1.64 \times 10^{-10}$$

$$\hat{r}_{\text{NiCo}} = (7.02 \times 10^{-9}) (0.5) - (2.06 \times 10^{-14}) (0.2) = 3.51 \times 10^{-9}$$

The rate of carbon diffusion was operated at temperature 1000 K and calculated via the Matlab software through the following equation

$$\bar{r} = f_1 \hat{r}_1 + f_2 \hat{r}_2 + f_3 \hat{r}_3$$

Where  $\bar{r}$  is the summary rate of carbon diffusion,  $f_i$  is the surface fraction of each metal and  $\hat{r}_i$  is the rate of carbon diffusion of each pure catalyst.

For example,  $\bar{r}$  at the middle step can be calculated as the above equation:  
content of Ni equal to 0.2, the content of Ni equal to 0.2, and content of NiCo equal  
to 0.6

$$\bar{r} = (0.76 \times 10^{-10})(0.2) + (1.64 \times 10^{-10})(0.2) + (3.51 \times 10^{-9})(0.6) = 2.15 \times 10^{-9}$$



## APPENDIX D

## MATLAB CODE FOR RATE OF COKE DIFFUSION CALCULATION

1. Declare parameters

```
syms fracNi fracCo fracNiCo fNi fCo fNiCo
```

```
syms thetaf thetar thetaselect
```

```
syms rateNi_f rateCo_f rateNiCo_f mixrate_f logmixrate_f logmixrate_r
```

2. Specify rate constant

```
KfNi = 3.71e+10;
```

```
KrNi = 5.49e+10;
```

```
KfCo = 4.88e+10;
```

```
KrCo = 4.00e+10;
```

```
KfNiCo = 5.76e+11;
```

```
KrNiCo = 1.17e+12;
```

3. Specify the surface coverage

```
Thetaf = [0.1, 0.5, 0.5];
```

```
Thatar = [0.0, 0.3, 0.5];
```

```
thetaselect = 3;
```

4. Calculation of forward rate of coke diffusion

```
P = 0;
```

```
for i = 1:size(fracNi,2)
```

```
    for j = 1:(size(fracCo,2)+1-i)
```

```
        [i,j];
```

```
    P = P+1;
```

```
    fNi(P) = fracNi(i);
```

```
    fCo(P) = fracCo(j);
```

```
    fNiCo(P) = (1-fracNi(i)-fracCo(j));
```

```
    rateNi_f(P) = KfNi*thetaf(thetaselect);
```



```

rateCo_f(P) = KfCo*thetaf(thetaselect);
rateNiCo_f(P) = KfNiCo*thetaf(thetaselect);
mixrate_f(P) = rateNi_f(P)*fNi(P) + rateCo_f(P)*fCo(P) + rateNiCo_f(P)*fNiCo(P);
logmixrate_f(P) = log10(mixrate_f(P));

rateNi_r(P) = KrNi*thetar(thetaselect);
rateCo_r(P) = KrCo*thetar(thetaselect);
rateNiCo_r(P) = KrNiCo*thetar(thetaselect);
mixrate_r(P) = rateNi_r(P)*fNi(P) + rateCo_r(P)*fCo(P) + rateNiCo_r(P)*fNiCo(P);
logmixrate_r(P) = log10(mixrate_r(P));

rateNi_rf(P) = KfNi*thetaf(thetaselect) - KrNi*thetar(thetaselect);
rateCo_rf(P) = KfCo*thetaf(thetaselect) - KrCo*thetar(thetaselect);
rateNiCo_rf(P) = KfNiCo*thetaf(thetaselect) - KrNiCo*thetar(thetaselect);
mixrate_rf(P) = rateNi_rf(P)*fNi(P) + rateCo_rf(P)*fCo(P) + rateNiCo_rf(P)*fNiCo(P);

    if mixrate_rf(P)>0
        logmixrate_rf(P) = log10(mixrate_rf(P));
    else
        logmixrate_rf(P) = -10;
    end

end

end

end

```

## REFERENCES

1. Böhringer, W., et al., *Selective Fischer-Tropsch Wax Hydrocracking—Opportunity for Improvement of Overall Gas-to-Liquids Processing*, in *Studies in Surface Science and Catalysis*, B.H. Davis and M.L. Occelli, Editors. 2007, Elsevier. p. 345-365.
2. Yue, L., et al., *Thermal-stable Pd@mesoporous silica core-shell nanocatalysts for dry reforming of methane with good coke-resistant performance*. *Fuel*, 2018. **218**: p. 335-341.
3. Wang, B., L. Song, and R. Zhang, *The dehydrogenation of CH<sub>4</sub> on Rh(111), Rh(110) and Rh(100) surfaces: A density functional theory study*. *Applied Surface Science*, 2012. **258**(8): p. 3714-3722.
4. Shamsi, A., *Methane Dry Reforming over Carbide, Nickel-Based, and Noble Metal Catalysts*, in *CO<sub>2</sub> Conversion and Utilization*. 2002, American Chemical Society. p. 182-196.
5. Xiaobo, B.A.I., et al., *Influence of Operating Conditions on Carbon Deposition Over a Ni Catalyst for the Production of Synthetic Natural Gas (SNG) from Coal*. *Catalysis letters*, 2014. **144**(12): p. 2157-2166.
6. Liu, A., S. Praserthdam, and S. Phatanasri, *Investigation on the increased stability of the Ni–Co bi-metallic catalysts for the carbon dioxide reforming of methane*. *Catalysis Today*, 2019.
7. Horlyck, J., et al., *Elucidating the impact of Ni and Co loading on the selectivity of bimetallic NiCo catalysts for dry reforming of methane*. *Chemical Engineering Journal*, 2018. **352**: p. 572-580.
8. Sauer, J., *Ab Initio Calculations for Molecule–Surface Interactions with Chemical Accuracy*. *Accounts of Chemical Research*, 2019. **52**(12): p. 3502-3510.
9. Habashi, F., *Nickel, Physical and Chemical Properties*, in *Encyclopedia of Metalloproteins*, R.H. Kretsinger, V.N. Uversky, and E.A. Permyakov, Editors. 2013, Springer New York: New York, NY. p. 1520-1520.
10. Habashi, F., *Cobalt, Physical and Chemical Properties*, in *Encyclopedia of Metalloproteins*, R.H. Kretsinger, V.N. Uversky, and E.A. Permyakov, Editors. 2013, Springer New York: New York, NY. p. 682-684.
11. Friend, D., J. Ely, and H. Ingham, *Thermophysical Properties of Methane*. *Journal of Physical and Chemical Reference Data - J PHYS CHEM REF DATA*, 1989. **18**: p. 583-638.
12. Praserthdam, S. and P.B. Balbuena, *Performance evaluation of catalysts in the dry reforming reaction of methane via the ratings concept*. *Reaction Kinetics, Mechanisms and Catalysis*, 2017. **122**(1): p. 53-68.
13. Argyle, M.D. and C.H. Bartholomew, *Heterogeneous Catalyst Deactivation and Regeneration: A Review*. *Catalysts*, 2015. **5**(1): p. 145-269.
14. Argyle, M. and C. Bartholomew, *Heterogeneous Catalyst Deactivation and Regeneration: A Review*. *Catalysts*, 2015. **5**: p. 145-269.
15. Lewars, E.G., *Computational Chemistry: Introduction to the Theory and Applications of Molecular and Quantum Mechanics*. 2011. 1-664.
16. Schlegel, H., *Exploring potential energy surfaces for chemical reactions: An overview of some practical methods*. *Journal of computational chemistry*, 2003. **24**: p. 1514-27.
17. Tsyganok, A.I., et al., *Dry reforming of methane over supported noble metals: a novel approach to preparing catalysts*. *Catalysis Communications*, 2003. **4**(9): p. 493-498.

18. Son, I.H., et al., *Study on coke formation over Ni/ $\gamma$ -Al<sub>2</sub>O<sub>3</sub>, Co-Ni/ $\gamma$ -Al<sub>2</sub>O<sub>3</sub>, and Mg-Co-Ni/ $\gamma$ -Al<sub>2</sub>O<sub>3</sub> catalysts for carbon dioxide reforming of methane*. *Fuel*, 2014. **136**: p. 194-200.
19. Bian, Z., et al., *Cover Feature: A Review on Bimetallic Nickel-Based Catalysts for CO<sub>2</sub> Reforming of Methane (ChemPhysChem 22/2017)*. *ChemPhysChem*, 2017. **18**(22): p. 3088-3088.
20. Niu, J., et al., *New mechanism insights into methane steam reforming on Pt/Ni from DFT and experimental kinetic study*. *Fuel*, 2020. **266**: p. 117143.
21. Praserthdam, S. and P.B. Balbuena, *Evaluation of dry reforming reaction catalysts via computational screening*. *Catalysis Today*, 2018. **312**: p. 23-34.
22. Galperin, F.M., *Magnetic moments of Fe, Co and N*. *Physics Letters A*, 1969. **28**(10): p. 667.
23. van Helden, P., et al., *Cobalt-nickel bimetallic Fischer-Tropsch catalysts: A combined theoretical and experimental approach*. *Catalysis Today*, 2020. **342**: p. 88-98.
24. Fuller, T., *Proton Exchange Membrane Fuel Cells 8*. 2008: Electrochemical Society.





จุฬาลงกรณ์มหาวิทยาลัย  
**CHULALONGKORN UNIVERSITY**



## REFERENCES



จุฬาลงกรณ์มหาวิทยาลัย  
**CHULALONGKORN UNIVERSITY**



จุฬาลงกรณ์มหาวิทยาลัย  
**CHULALONGKORN UNIVERSITY**

## VITA

NAME Mogkol Lerdpongsiripaisarn  
DATE OF BIRTH 9 August 1996  
INSTITUTIONS ATTENDED Chulalongkorn University  
HOME ADDRESS 24/17 Thungyao, Palian, Trang

